3-22-2019

Quantifying Uncertainty of Ensemble Transport and Dispersion Simulations Using HYSPLIT

Daniel W. Bazemore

Quantifying Uncertainty of Ensemble Transport and Dispersion Simulations Using HYSPLIT

THESIS

Daniel W. Bazemore, Captain, USAF

AFIT-ENP-MS-19-M-068

DEPARTMENT OF THE AIR FORCE
AIR UNIVERSITY

AIR FORCE INSTITUTE OF TECHNOLOGY

Wright-Patterson Air Force Base, Ohio

AFIT-ENP-MS-19-M-068

QUANTIFYING UNCERTAINTY OF ENSEMBLE TRANSPORT AND DISPERSION SIMULATIONS USING HYSPLIT

THESIS

Presented to the Faculty

Department of Engineering Physics

Graduate School of Engineering and Management

Air Force Institute of Technology

Air University

Air Education and Training Command

In Partial Fulfillment of the Requirements for the

Degree of Master of Science in Atmospheric Science

Daniel W. Bazemore, BS

Captain, USAF

21 March 2019

AFIT-ENP-MS-19-M-068

QUANTIFYING UNCERTAINTY OF ENSEMBLE TRANSPORT AND DISPERSION SIMULATIONS USING HYSPLIT

Daniel W. Bazemore, BS

Captain, USAF

Committee Membership:

H. Rose Tseng, Air Force Institute of Technology
Chair

Robert C. Tournay, Air Force Institute of Technology
Member

A. Suarez-Mullins, Air Force Technical Applications Center
Member

Abstract

Uncertainty associated with determining the source location of nuclear pollutants in the atmosphere after a nuclear fallout using a numerical model is difficult to determine. Uncertainty can originate from input data (meteorological and emissions), internal model error, physics parameterizations, and stochastic processes. This study uses the Hybrid Single Particle Lagrangian Integrated Trajectory (HYSPLIT) model with data from the 1983 Cross Appalachian Tracer Experiment (CAPTEX) (Ferber et al. 1986) and simulating six nuclear detonations (Rolph et al. 2014) to quantify and communicate uncertainty in ensemble dispersion simulations. This is accomplished by utilizing an ensemble of forward trajectory simulations varying initial conditions and physical parameterizations (e.g. turbulence, boundary layer stability and mixed layer depth). The model rank for each simulation is calculated using ground measurements. This value is compared against the observed rank from the CAPTEX experiment to measure the sensitivity of each model run. Effectively quantifying and communicating uncertainty is crucial in providing probabilistic results in nuclear monitoring.

Acknowledgments

This thesis was not completed through the sole efforts of one individual, but through the contributions of many. I could not have done this work without the support of the following individuals; therefore I offer my heartfelt appreciation to:

Lt Col Tournay (USAF) for his mentorship during this endeavor, and for serving on my committee.

Lt Col Stubblefield (USAF) for his mentorship and support in helping me pursue this degree. He has played a pivotal role in my development as an Air Force officer.

Major Rose Tseng (USAF) for her time, knowledge, and most importantly guidance while serving as my research advisor. She led and encouraged me through this journey. This document is part of her legacy as an Air Force officer, instructor, and fellow scientist. Go, Confront the Problem, Fit, Win!

Major Omar Nava (USAF) for his instruction and guidance not only during this project, but during the courses that laid the groundwork for this research. His ideas and direction made the coding required in this project possible.

Dr. Suarez-Mullins (AFTAC) for her support and advice throughout the research process.

Air Resources Laboratory (ARL) for access to HYSPLIT and data.

My classmates: Their support and willingness to assist me when I was stuck on a challenge has not gone unnoticed. We have completed this journey together; I look forward to working/serving with you in the future. As with Homework 3, you will not be forgotten.

My success is made possible first and foremost by God, and secondly from the teachings and assistance of my **parents**. To my fiancé for her encouragement and support. To my **siblings** for their love and prayers; they have always and will continue to be my best friends and biggest fans. Although we might be separated geographically, we remain as close as we have ever been…only a phone call away.

Table of Contents

List of Figures

List of Tables

List of Acroynoms

AFPT	ARL Fallout Prediction Technique
ARL	Air Resource Laboratory
BL	boundary layer
CAPTEX	Cross Appalachian Tracer Experiment
CC	correlation coefficient
DOE	Department of Energy
FB	fractional bias
FMS	figure of merit in space
HYSPLIT	HYbrid Single-Particle Lagrangian Integrated Trajectory
KSP	Kolmogorov-Smirnov Parameter
kT	kiloton
MCF	Meteorology Complex Factor
ML	mixing layer
MLCAPE	mixed layer convective available potential energy
MRF	Medium-Range Forecast
MSL	mean sea level
NATO	North Atlantic Treaty Organization
NCAR	National Center for Atmospheric Research
NCEP	National Center for Environmental Prediction
NH	New Hampshire
NJ	New Jersey
NOAA	National Oceanic & Atmospheric Administration

NRTS	National Reactor Testing Station
NWP	numerical weather prediction
NWS	National Weather Service
NY	New York
OH	Ohio
ON	Ontario
PA	Pennsylvania
PBL	planetary boundary layer
PMCH	perfluoro-monomethyl-cyclohexane
RI	Rhode Island
SPS	Special Project Section
TKE	turbulent kinetic energy
UTC	Universal Time Coordinated
VAFTAD	Volcanic Ash Forecast & Dispersion
VT	Vermont
WRF	Weather Research & Forecasting
YSU	Yonsei University

QUANTIFYING UNCERTAINTY OF ENSEMBLE TRANSPORT AND DISPERSION SIMULATIONS USING HYSPLIT

Introduction

General Issue

Atmospheric transport and dispersion models aim to mathematically estimate the behavior of pollutants or contaminates in the atmosphere. These contaminates include, but are not limited to, toxic gases, radionuclide, volcanic ash, and other anthropogenic or organic aerosols. The use of transport and dispersion models can be applied to macrobiotic aerosols; however, these models are of great importance to predict the movement of airborne radionuclides for emergency response preparedness. Particulates or gasses released during the testing of nuclear explosives and the toxins released from nuclear reactor accidents such as Chernobyl or Fukushima pose a significant threat to public health. Although modeling these hazards has advanced significantly in the past 80 years, few efforts have proven fruitful to quantify error in these simulations.

Problem Statement

Outcomes from transport and dispersion modeling are subject to a varying degree of uncertainties that are difficult to quantify. These uncertainties stem from meteorological processes (dependent on meteorology model ingested into the model), internal modeling error, and stochastic processes. Most notably, the fundamental uncertainty of any transport and dispersion model stems from the parameterizations found within its core. These parameterizations seek to characterize the physical environment that are either too complex to be resolved or not sufficiently understood (Stensrud 2007). Parameterization schemes are important because they significantly

influence model generated forecasts and interact with one other indirectly though their changes to model variables (Stensrud 2007). One of the most valuable tools to expose this type of uncertainty is through the use of ensembles. This paper seeks to highlight the factors that lead to some of the uncertainty of atmospheric transport and dispersion modeling by utilizing an ensemble of forward trajectory simulations with varying initial conditions and physical parameterizations (e.g. turbulent velocity, boundary layer stability and mixed layer depth).

Hypotheses

It is hypothesized uncertainty in atmospheric dispersion model predictions is associated with: 1) the data ingested into the model, 2) model parameterizations, and 3) the stochastic uncertainty associated with the turbulent nature of the atmosphere. The data ingested into the model introduces a varying level of uncertainty. This uncertainty is assumed to be linked to the horizontal and vertical resolution of the dataset (Rao 2005). In this experiment, it is hypothesized finer meteorological model data resolutions more accurately predicts the location and timing of pollutants compared to more coarse resolutions. Uncertainty also stems from inaccurate treatment of the dynamical and chemical processes parameterized within the model (Rao 2005). Due to the relatively short term nature of the simulations it is assumed the boundary layer stability and turbulence parameterizations will have the greatest effect on uncertainty. The uncertainties associated with the data and parameterizations can be minimized by using more accurate and representative measurements and improving model dynamics and parameterization schemes (Rao 2005). The final factor impacting uncertainty, the

stochastic nature of the atmosphere, cannot be minimized by any actions taken by scientists because it arises from the natural variability of the atmosphere (Rao 2005).

Research Objective, Focus and Questions

This research aims to:

1. Quantify uncertainty in the long-range atmospheric trajectory and dispersion modeling for Cross-Appalachian Tracer Experiment Release 2 (CAPTEX2).

The model in question is the National Oceanic and Atmospheric Administration (NOAA) Air Resources Laboratory's (ARL) Hybrid Single-Particle Lagrangian Integrated Trajectory (HYSPLIT) model. Output from an ensemble of the model is compared against the atmospheric concentrations of a tracer experiment released in the northeast United States and southeast Canada, called the Cross-Appalachian Tracer Experiment (CAPTEX '83). The use of five statistical values: Figure of Merit in Space, Correlation Coefficient, Fractional Bias, Kolmogorov-Smirnov, and Final Rank are used to compare the CAPTEX measured and HYSPLIT predicted concentration values. These statistics are used to quantify the uncertainty of the spatial extent of the plume. Furthermore, the onset time of the plume at sixty-eight stations from CAPTEX is compared to the onset timing computed by the model at the same locations. This timing difference is used to quantify the temporal uncertainty of the plume.

2. Quantify uncertainty in nuclear detonations atmospheric trajectory and dispersion modeling.

HYSPLIT output is compared against the atmospheric concentrations from the fallout of stabilized nuclear clouds. The nuclear fallouts are from six detonations tested at the Nevada Test site between 1951 and 1957 (Rolph et al. 2014). The five statistical

values mentioned above are calculated for an ensemble of each nuclear detonations and compared to measured concentrations. Due to the short time span of a stabilized nuclear detonation simulation, quantifying uncertainty places emphasis on the figure of merit in space.

Preview

The organization of this thesis is as follows: Chapter II describes the background on the CAPTEX and nuclear fallout from the Nevada Test site data, the history of HSYPLIT and explains model calculations and parameterizations; Chapter III describes the methodology for this research; Chapter IV presents and analyses the results; Chapter V discusses the impacts of this work and concludes this research by presenting recommendations for future work in this field.

II. Background & Literature Review

Chapter Overview

The purpose of this chapter is to provide background information on the data used, procedures practiced, and modeling capabilities utilized in this research. This chapter outlines the state of current and relevant research critical to understand the findings and conclusions.

Cross Appalachian Tracer Experiment

The Cross-Appalachian Tracer Experiment (CAPTEX) was a large scale, bi-national field study conducted in 1983, the purpose of which was three-fold: 1) it aimed to test tracer technology on a 1000-km scale, 2) provide insight into the mechanisms involved in long-range transport and dispersion, and 3) provide data to evaluate and improve transport and dispersion modeling (Ferber et al. 1986). The experiment was conducted from mid-September through October of 1983 across the northeastern United States and southeastern Canada. Research was directed by the National Oceanic and Atmospheric Administration's (NOAA) Air Resources Laboratory (ARL) in association with scientists from the National Weather Service (NWS) and Department of Energy (DOE).

Research began with the development of a tracer system suitable for the long-range atmospheric dispersion experiments. The chemically and biologically inert perfluoro-monomethyl-cyclohexane ([PMCH]: C_7F_{14}) served as the tracer for the experiment. In its basic state, PMCH is a clear, colorless liquid and is thermally stable up to extreme temperatures (400ºC) (Ferber et al. 1986). When released as a gas, PMCH is harmless and can be accurately measured at extremely low concentrations (3 parts per

10^{15} parts of air). Before release, the PMCH was vaporized and mixed with a stream of nitrogen to ensure the tracer was capable of being carried through the atmosphere (Ferber et al. 1986). The N_2-PMCH mixture was fully vaporized using a tube furnace kept at 105º C. From the tube the gas passed through a mass flowmeter where the volume was measured and recorded on a flowmeter totalizer and stripchart recorder. The tracer reservoir was weighed using both crane scales (capable of measuring 0 – 454 kg) and small balances (0 – 40 kg) before and after each release to provide a system of checks on the total amount released (Ferber et al.1986).

In total CAPTEX was composed of six tracer releases: four from Dayton, Ohio, and two from Sudbury, Ontario. These locations are identified as key pollutant source areas that have a significantly adverse effect on air quality in the northeastern United States and southeastern Canada (Ferber et al. 1986). The tracer was released at 10 meters above ground level for three consecutive hours. The Dayton releases were conducted in the early afternoon to ensure the tracer was vertically well-mixed such that the large scale wind pattern advected the tracer over the sampling network. The Sudbury releases occurred in the early morning hours after the passage of cold fronts that provided northwesterly winds which brought the plume over the sampling networks.

After release, automatic sequential air samplers at 86 ground stations collected six consecutive air samples ranging from three to six hours long. The sampling sites were located in approximately 100-km arc intervals from the source location, ranging from 300 km to 1100 km (Figure 1). The first number in the three digit site identifier represents the distance on the arc away from Dayton in hundreds of kilometers. The remaining two digits represent the position along the arc from south to north. The spacing of the

samplers along each arc was approximated based on an expected two plume standard deviations pattern (Ferber et al.1986). The spacing increases linearly with distance from the release site. The number of sampling locations on the 800-km arc was doubled to provide more detailed plume structure. In total, nearly 3000 samples were collected from the network of ground stations.

For this research, the second CAPTEX release (CAPTEX2) was chosen as the verification for the computer model simulations. CAPTEX2 was released at Dayton International Airport (39.90ºN, 84.05ºW) on September 25, 1983. 201 kg of PMCH was released from 1705-2005 UTC and measured at 68 sites across the northeast United States and southeast Canada (Table 1). Focus is placed on CAPTEX2 to thoroughly investigate the uncertainty.

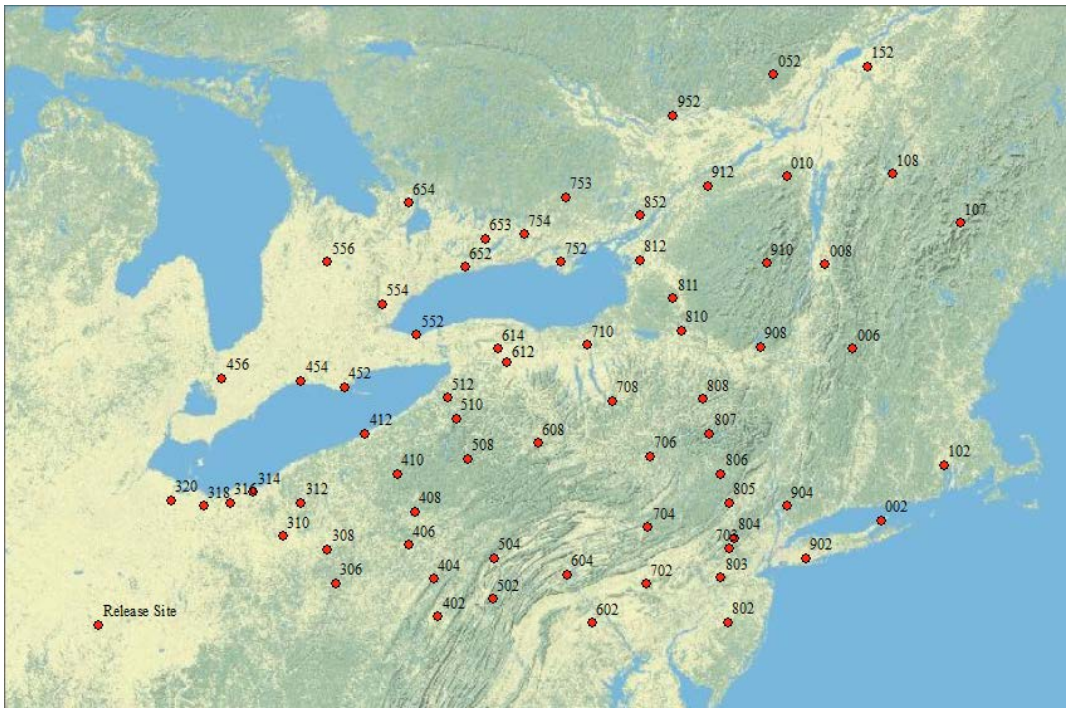

Figure 1: Network of ground based sensors from the CAPTEX2 experiment. Release site of CAPTEX2 was Dayton, Ohio.

Table 1. CAPTEX2 Sampling Sites				
Site #	Site Name	Elevation (m, MSL)	Latitude (ºN)	Longitude (ºW)
306	Steubenville, OH	303	40.38	-80.63
308	Lisbon, OH	333	40.77	-80.75
310	Akron-Canton AP, OH	369	40.92	-81.43
312	Hiram, OH	375	41.30	-81.15
314	Cleveland, OH	235	41.42	-81.87
316	Oberlin, OH	249	41.30	-82.22
318	Norwalk, OH	204	41.27	-82.62
320	Fremont, OH	183	41.33	-83.12
402	Somerset, PA	640	40.00	-79.08
404	Blairsville, PA	561	40.43	-79.15
406	Kittanning Lock, PA	241	40.82	-79.53
408	Clarion, PA	340	41.20	-79.43
410	Titusville, PA	372	41.63	-79.70
412	Erie, PA	223	42.08	-80.18
452	Long Point, ON	175	42.60	-80.5
454	Port Stanley, ON	213	42.67	-81.15
456	Wilkesport, ON	183	42.70	-82.35
502	Saxton, PA	238	40.20	-78.25
504	Tyrone, PA	265	40.67	-78.23
508	Bradford, PA	652	41.80	-78.63
510	Little Valley, NY	480	42.25	-78.8
512	Gowanda, NY	262	42.48	-78.93
552	Vineland, ON	79	43.18	-79.40
554	Milton, ON	221	43.52	-79.92

Site #	Site Name	Elevation (m, MSL)	Latitude (ºN)	Longitude (ºW)
602	York, PA	119	39.92	-76.75
604	Newport, PA	116	40.48	-77.13
608	Westfield, PA	61	41.98	-77.57
612	Pavilion, NY	287	42.88	-78.03
614	Batavia, NY	278	43.03	-78.18
652	Bowmanville, ON	99	43.92	-78.67
653	Peterborough A., ON	191	44.23	-78.37
654	Coldwater, ON	280	44.62	-79.53
702	Reading, PA	82	40.37	-75.93
703	Chester, NJ	289	40.78	-74.67
704	Freeland, PA	580	41.02	-75.90
706	Montrose, PA	475	41.83	-75.87
708	Ithaca, NY	293	42.45	-76.45
710	Clyde, NY	128	43.07	-76.83
752	Bloomfield, ON	91	43.98	-77.22
753	Kaladar, ON	244	44.68	-77.15
754	Campbellford, ON	175	44.28	-77.78
802	Pemberton, NJ	16	39.93	-74.70
803	Wertsville, NJ	49	40.45	-74.80
804	West Wharton, NJ	223	40.90	-74.6
805	High Point Park, NJ	430	41.30	-74.67
806	Mongaup Valley, NY	380	41.63	-74.80
807	Downsville Dam, NY	396	42.08	-74.97
808	Oneonta, NY	427	42.47	-75.07
810	Griffiss AFB, NY	148	43.23	-75.40

Site #	Site Name	Elevation (m, MSL)	Latitude (ºN)	Longitude (ºW)
812	Watertown, NY	97	44.00	-76.02
852	Charleston Lake, ON	92	44.48	-76.03
902	Merrick, NY	6	40.67	-73.52
904	Yorktown Heights, NY	204	41.27	-73.80
908	Broadalbin, NY	256	43.05	-74.20
910	Newcomb, NY	506	43.97	-74.10
912	Norfolk, NY	70	44.80	-75.00
952	Angers, ON	94	45.55	-75.52
102	Providence, RI	16	41.73	-71.43
107	Gorham, NH	261	44.40	-71.18
108	Newport, VT	234	44.93	-72.20
152	St. Zephirin, ON	52	46.07	-72.58
002	Greenport, NY	5	41.10	-72.37
006	Wardsboro, VT	424	43.03	-72.80
008	Cornwall, VT	150	43.95	-73.22
010	Ellenburg Depot, NY	262	44.90	-73.80
052	St. Hyppolite, ON	366	45.98	-74.00

Table 1: CAPTEX 2 ground measurement sites (Ferber et al. 2014)

High pressure over the northeastern United States controlled the meteorological conditions during CAPTEX2. Light winds across the eastern United States forced the plume to disperse widely across the northeast United States and southeast Canada (Figure 2).

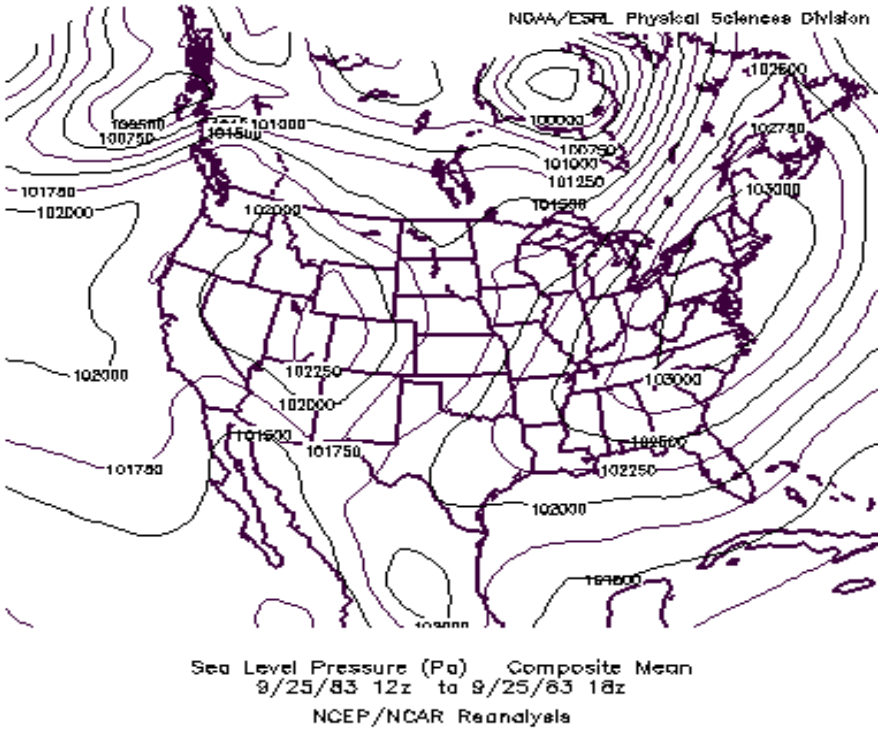

Figure 2: Sea level pressure at the surface average between 12Z and 18Z on 25 September 1983 across the United States. The CAPTEX 2 plume was released at 1705Z. A high pressure system was positioned over the eastern United States with light winds aloft which allowed the plume to disperse widely across the receptor field (Earth System Research Laboratory 2019).

Nuclear Detonation Cases

CAPTEX data is useful to quantify uncertainty of atmospheric transport and dispersion on large scale synoptic flow (~1100 km); however CAPTEX doesn't necessarily represent the environmental conditions of a nuclear detonation. For this reason, the second goal of this project is to complete an ensemble for six nuclear detonations to test the sensitivity of model parameterizations on detonation environments.

In total, the United States conducted 928 atmospheric underground nuclear tests at the Nevada Test Site between 1951 and 1992 (Rolph et al. 2014). The Nevada Test Site, a 1375 square mile stretch of desert located 90 miles northwest of Las Vegas, Nevada, is owned and operated by the Department of Energy. For the purpose of this research, six

nuclear detonations are simulated by HYSPLIT (Figure 3). These six cases were chosen based upon their relatively small nuclear yield (<50 kT) and proximity to the surface. All were detonated close to, but above, the surface except Buster-Jangle Sugar which was detonated at the surface (Rolph et al. 2014). Furthermore, these six cases produced pollutant plume that stretched far downwind, which made them ideal to test the uncertainty of the dispersion of these clouds.

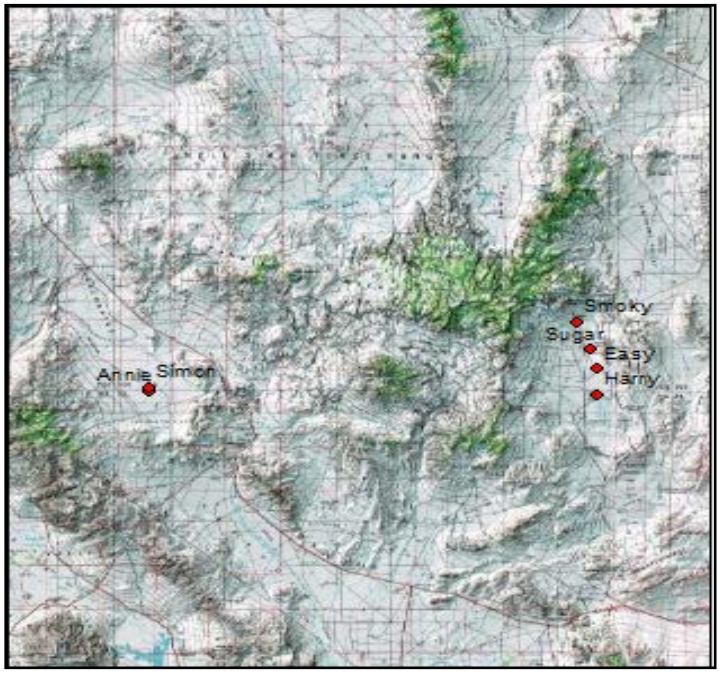

Figure 3: Nuclear experiment Sugar (1.2 kT yield), Easy (12 kT), Annie (16 kT), Harry (32 kT), Simon (43 kT), and Smoky (44 kT) test sites (Earth System Research Laboratory 2019).

Buster-Jangle Sugar Shot

The first and smallest nuclear detonation used in this study was the Buster-Jangle Sugar shot. This 1.2-kiloton (kT) device was detonated at 1700 UTC on November 19, 1951. The cloud produced by the detonation reached 4572 m mean sea level (MSL) and created a crater 6 m deep and 27 m across (Rolph et al. 2014). At the time of detonation, a high pressure system was located to the east in Colorado (Figure 4) with a low pressure

center off northwestern United Sates (not depicted on figure). Surface winds were reported at 1 m/s from the south, 16 m/s from the south-southwest at 3200 m MSL, and 21 m/s from the south-southwest at 4250 m MSL.

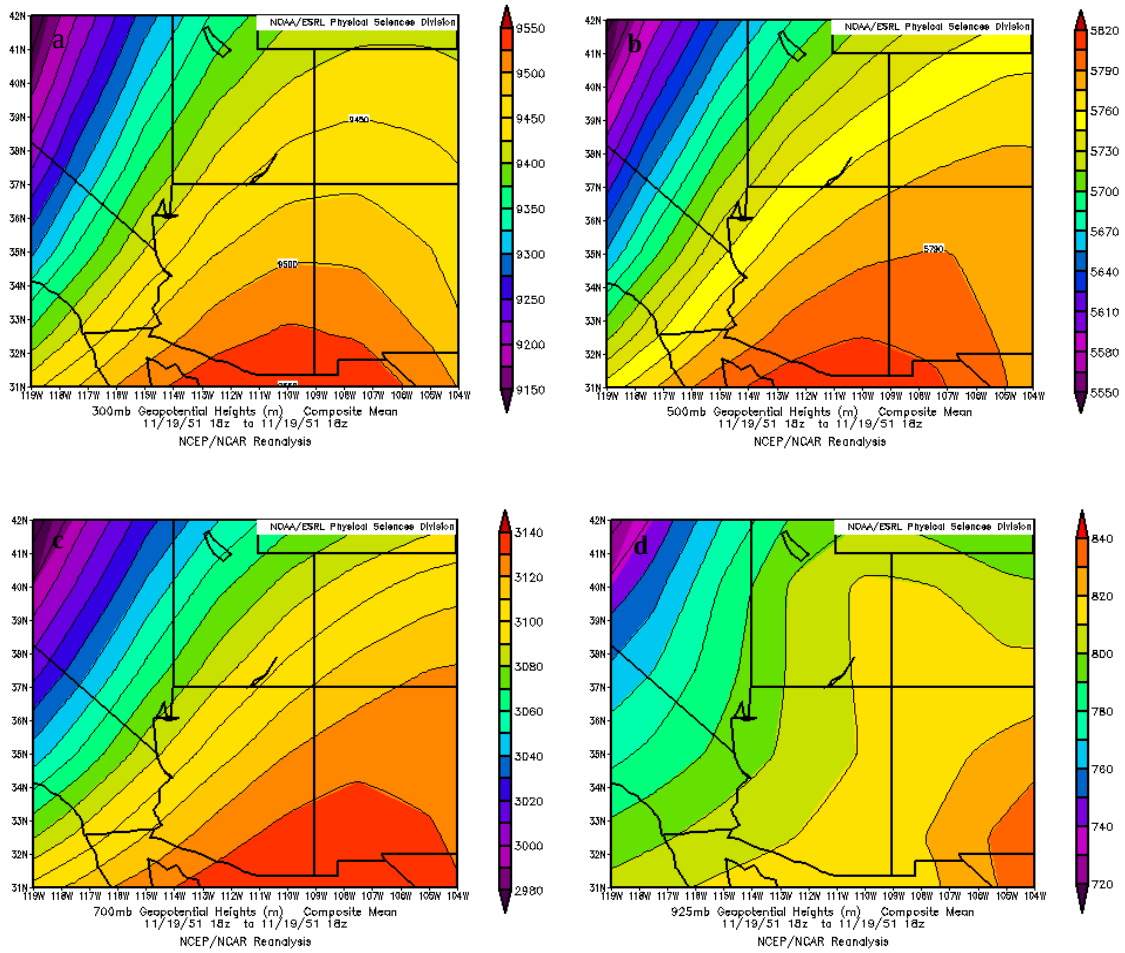

Figure 4: Geopotential heights in meters from the NCAR/NCEP Reanalysis dataset at the (a) 300-hPa, (b) 500-hPa, (c) 700-hPa, and (d) 925-hPa at the time of the Sugar detonation (19 November 1951 at 1700 UTC).

Tumbler-Snapper Easy Shot

The second nuclear detonation, Tumbler-Snapper Easy, occurred on May 7, 1952 at 1215 UTC. This 12-kT detonation was conducted from a 91-m tower and produced a plume that extended 10 km MSL. Winds near the surface were calm at the time of

detonation, 18 m/s from the south at 3000 m MSL, and from the south-southwest at 34 m/s at 5800 m MSL. As the day progressed, winds at the surface increased with occasional gusts of 25 m/s. Light precipitation associated with a stationary front and low-pressure system in the area was reported in the region, including the regions where the plume extended (Figure 5).

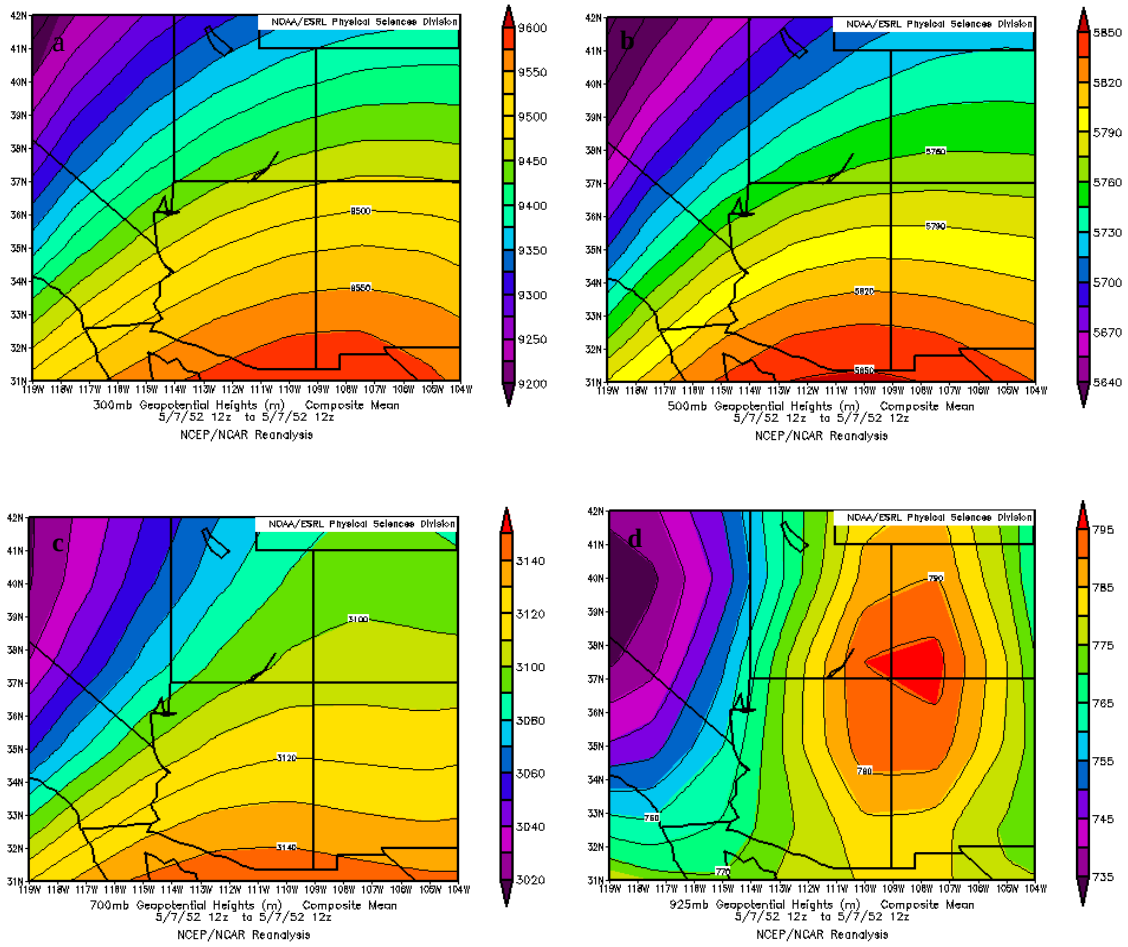

Figure 5: Geopotential heights in meters from the NCAR/NCEP Reanalysis dataset at the (a) 300-hPa, (b) 500-hPa, (c) 700-hPa, and (d) 925-hPa at the time of the Easy detonation (7 May 1952 at 1215 UTC).

Upshot-Knothole Annie Shot

On March 17, 1953, at 1320 UTC, Upshot-Knothole Annie was detonated from a 91-m tower. This 16-kT detonation was the first of elevation shots in the Upshot-Knothole Operation. The nuclear cloud tops was observed to reach an elevation of 12,500 m MSL. The test's intent was to study the effect of the nuclear blast on houses, automobiles and other man-made items (Rolph et al. 2014). At the time of detonation, the wind direction varied from southwest to the west from the surface up to 15,000 m MSL.

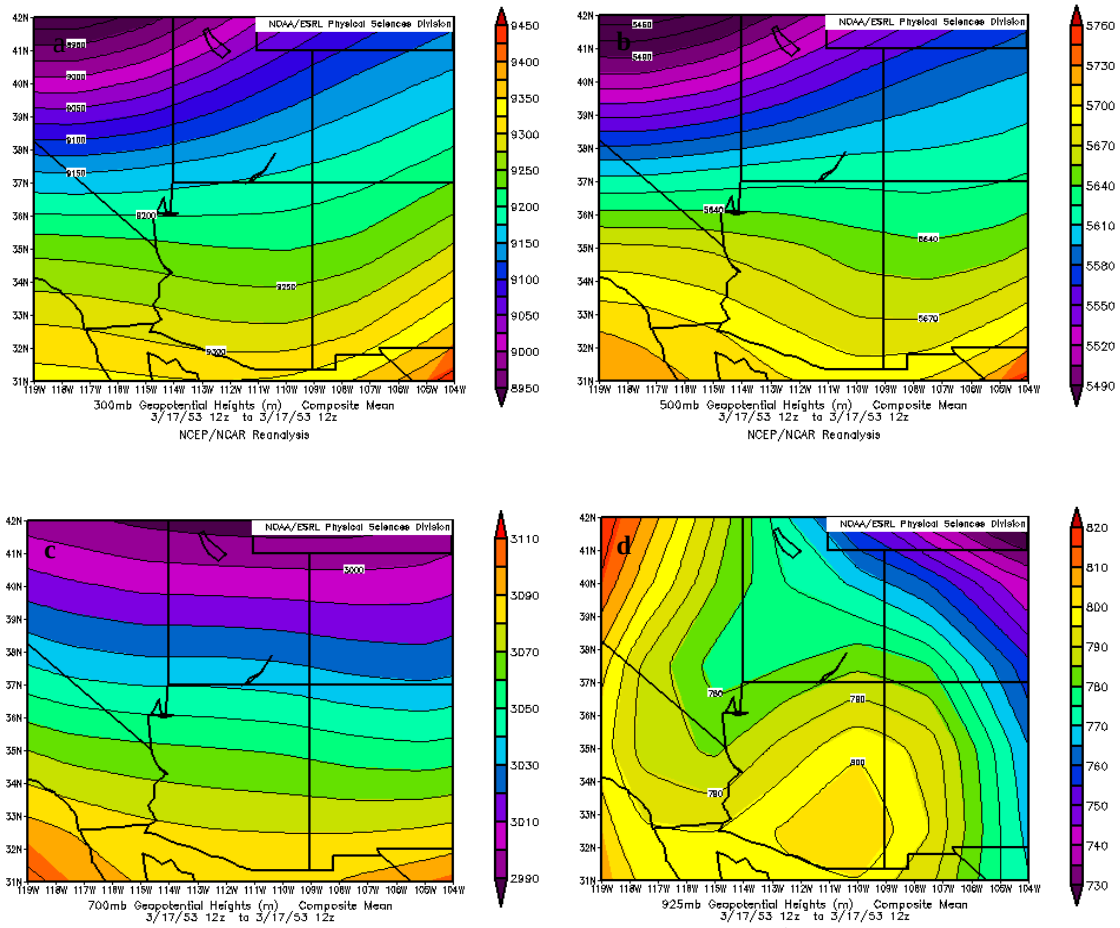

Figure 6: Geopotential heights in meters from the NCAR/NCEP Reanalysis dataset at the (a) 300-hPa, (b) 500-hPa, (c) 700-hPa, and (d) 925-hPa at the time of the Easy detonation (17 March 1953 at 1320 UTC).

The presence of a cold front near the Nevada Test Site led to a strong gradient of wind speed between 2500 m and 2700 m MSL; there were no reports of precipitation in the region (Figure 6).

Upshot-Knothole Simon Shot

Upshot-Knothole Simon occurred on April 25, 1953, at 1230 UTC. The 43-kT yield detonation was two and a half times the size of Annie and was one of the largest near-surface detonations ever at the Nevada Test Site. Like Annie, Simon was shot from a 91-m tower with cloud tops that reached 13,000 m MSL. Surface winds at the time of detonation were 3 m/s from the north-northwest with light winds extending up to 2,500 m MSL. Above 2,500 m MSL winds remained from the west-northwest increasing in speed throughout the column associated with an upper level low (Figure 7). There were no reports of precipitation. The sea level pressure at the surface indicates the test site was in a cull region at the time of the experiment (Figure 7).

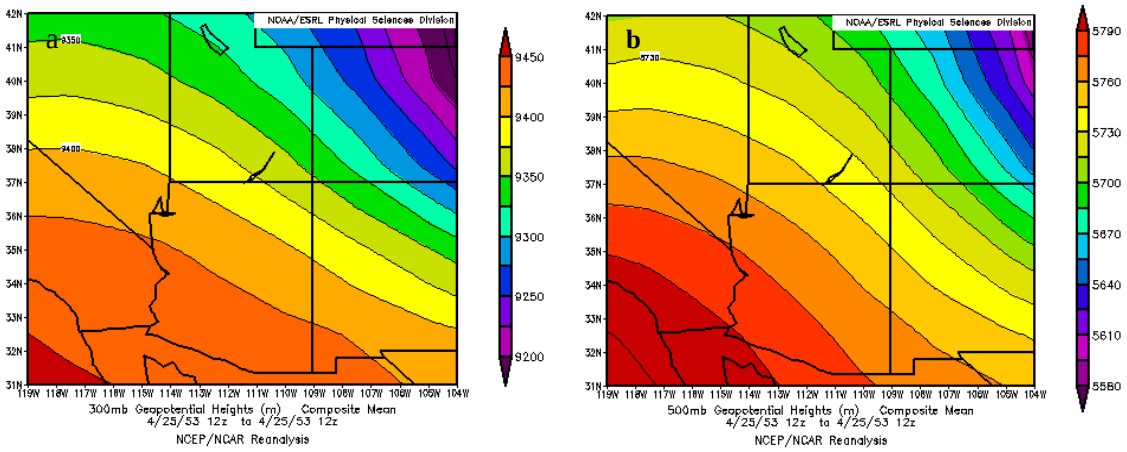

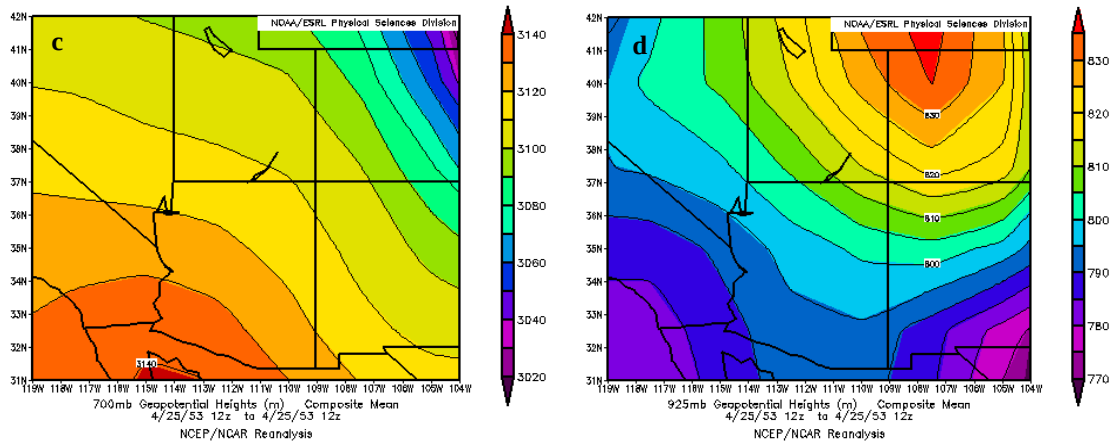

Figure 7: Geopotential heights in meters from the NCAR/NCEP Reanalysis dataset at the (a) 300-hPa, (b) 500-hPa, (c) 700-hPa, and (d) 925-hPa at the time of the Simon detonation (25 April 1953 at 1230 UTC).

Upshot-Knothole Harry Shot

The ninth of eleven shots in the Upshot-Knothole Operation was Harry. This 32-kT yield detonation was conducted on a 91-m tower on May 19, 1953, at 1205 UTC. The cloud from Upshot-Knothole Harry Shot reached 13,000 m MSL. At the time of launch, surface winds were from the north-northeast at 7 m/s. From the height of the burst to 4,500 m MSL wind speeds varied from 7 m/s to 13 m/s from the southwest. Above 4,500 m MSL winds were out of the west-northwest from 15 m/s to 40 m/s. There were no reports of precipitation over the test site; however there were reports of precipitation immediately downwind. It is believed this precipitation did not lead to deposition of the radioactive material directly downwind of the site; however in the northern and eastern extent of the plume deposition is believed to have occurred because of rainfall. The sea level pressure indicates a weak trough at the surface (Figure 8).

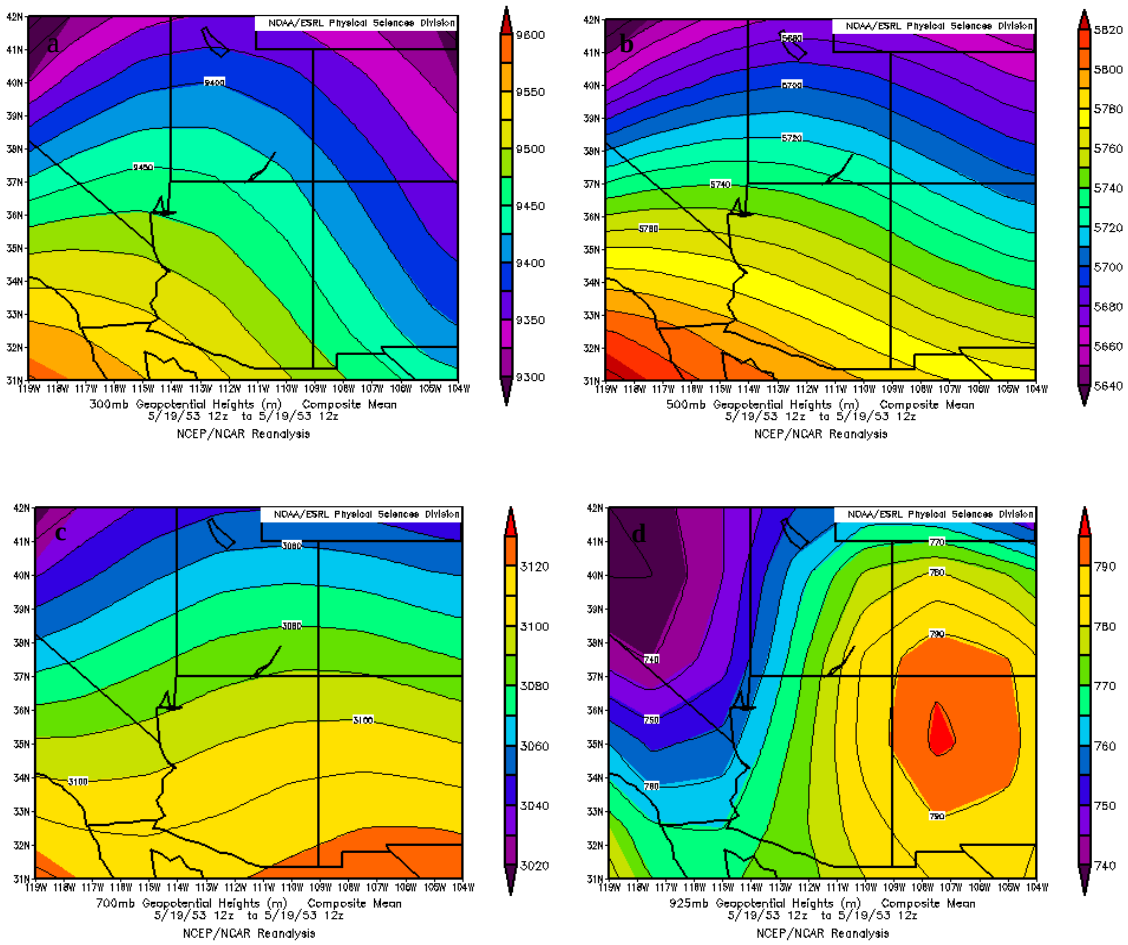

Figure 8: Geopotential heights in meters from the NCAR/NCEP Reanalysis dataset at the (a) 300-hPa, (b) 500-hPa, (c) 700-hPa, and (d) 925-hPa at the time of the Harry detonation (19 May 1953 at 1205 UTC).

Plumbbob Smoky Shot

The largest of the six detonation studied in this research was Plumbbob Smoky. This 44-kT detonation was conducted from a 195-m tower at 1230 UTC on August 31, 1957. Smoky was launched from this height in an attempt to minimize the amount of fallout immediately downwind of the launch site. At the time of the Smoky detonation, an upper level low was centered over northern Nevada and northern Utah (Figure 9). This low supported a 925-hPa low centered over the intersection of the borders of California,

Arizona, and Mexico. Winds below 1580 m MSL were calm with winds from 1580 m MSL to 4500 m MSL from the north at 2 m/s to 5 m/s. Winds above 4500 m MSL were reported from the west-northwest at 5 m/s to 25 m/s. There are no reports of precipitation at the test site; however, rain was reported downstream in the plume which is believed to contribute to deposition of the nuclear cloud.

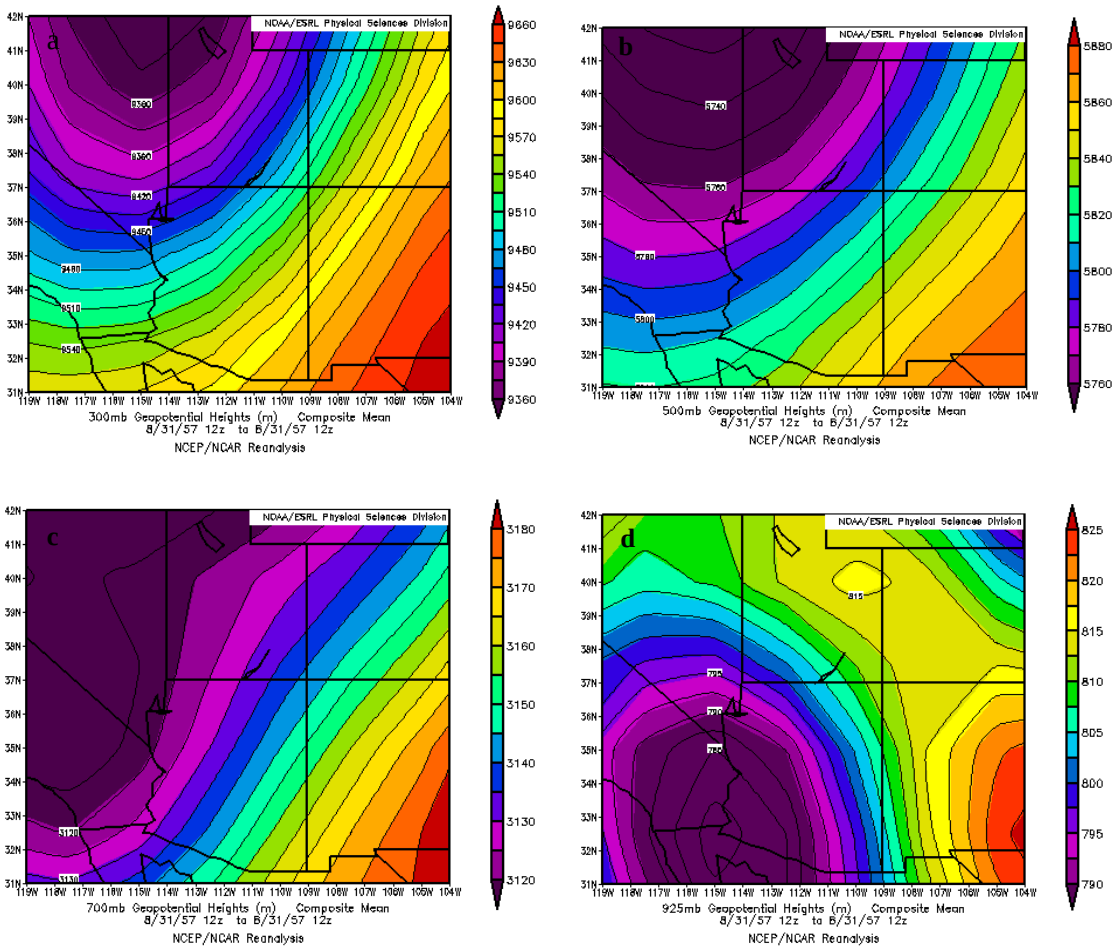

Figure 9: Geopotential heights in meters from the NCAR/NCEP Reanalysis dataset at the (a) 300-hPa, (b) 500-hPa, (c) 700-hPa, and (d) 925-hPa at the time of the Smoky detonation (31 August 1957 at 1230 UTC).

Meteorological Models

Model Background

Numerical weather prediction (NWP) models are computer software programs that employ physics-governing equations to describe fluid dynamics. These equations, combined with numerical methods and parameterizations, are used to characterize the current and future state of the atmosphere (Warner 2011). The first NWP models were simplified versions of the equations of motions and fluid dynamics and were applied to a small region of the globe (Stensrud 2007). The first of these models was created by Cahrney, Fyortolft, and von Neumann who produced a one-day forecast using a one-layer barotropic model. Over the next 70 years atmospheric scientists worked together to create and amend NWP models. Their goal was two-fold: 1) The first objective was to create models capable of predicting atmospheric conditions for communities across the globe, 2) Their second purpose was to create models for use by research communities to further their understanding of the atmosphere.

As with most atmospheric transport and dispersion models, HYSPLIT is sensitive to the accuracy and quality of the meteorological data ingested into the model. The available meteorological data model chosen for this research is the Weather Research and Forecasting Model (WRF).

Weather Research and Forecasting Model

The WRF Model is a non-hydrostatic mesoscale numerical weather prediction system created for both atmospheric research and operational forecasting applications (NCAR 2006). WRF contains physics parameterizations that are based on actual

atmospheric conditions. These parameterizations work together to simulate atmospheric behavior.

For the CAPTEX simulations, the WRF model, obtained from ARL, was configured with horizontal resolutions of 27-km, 9-km, 3-km (nested in the 9-km). The varying horizontal resolutions were used to test the sensitivity of atmospheric dispersion modeling on the resolution of the meteorological model ingested. This version of WRF 3.2 uses the Yonsei University (YSU) planetary boundary layer (PBL) scheme. This nonlocal scheme is like previously constructed schemes, such as the Medium-Range Forecast (MRF) Model scheme; however, YSU represents entrainment at the top of the PBL explicitly (Hong et al. 2006). The YSU scheme more accurately simulated deeper vertical mixing in buoyancy-driven boundary layer environments with shallower mixing in strong-wind regimes compared to other PBL schemes, such as the MRF scheme (Hong et al. 2006). On the other hand, the YSU over-deepens the PBL for springtime deep convective environments (Coniglio et al. 2013). In these environments the YSU scheme results in too much dry air near the surface and an underestimation of the mixed layer convective available potential energy (MLCAPE) in deep convective atmosphere conditions.

Pertaining to the nuclear detonation simulations, data from the global NCEP/NCAR Reanalysis Project (NNRP) is available. NNRP data is a product of the combined efforts between NOAA National Centers for Environmental Prediction (NCEP) and the National Center for Atmospheric Research (NCAR). NNRP data is on a 2.5º global latitude-longitude grid with a temporal resolution of six hours (Rolph et al.2014). Vertically, there are 17 pressure levels between 1000 hectopascals (hPa) and 10 hPa. The

data is originally in GRIB format; therefore it has been converted to a HYSPLIT compatible form.

Atmospheric Transport and Dispersion

The rate at which atmospheric transport and dispersion of pollutants occur is a product of three main meteorological processes. Immediately following release, pollutants are carried from their release site by the mean wind velocity field (Draxler and Hess 1988). As the plume progresses through the atmosphere, smaller-scale turbulent processes within the mean wind flow work to disperse the pollutant (Draxler and Hess 1988). The final force affecting the plume is the process of deposition. Deposition is classified into two overarching types: dry or wet. Dry deposition is the process by which atmospheric gases and particles are transferred to the surface as a result of random turbulent air motions and sedimentation (Wesley 1989). Wet deposition is defined as the removal of atmospheric gases or particles through their incorporation into hydrometeors, which are then lost by precipitation (Draxler and Hess 1998). Transport and dispersion models vary on how they handle these processes depending on their complexity and assumptions. The two most common modeling schemes to compute the time history of air pollutant concentrations are the Eulerian and Lagrangian approaches (Draxler and Hess 1998). The type of contamination scenario often dictates which framework is more advantageous.

Eulerian models aim to solve for the advection and diffusion of a pollutant in a single equation on a fixed grid. This approach is typically applied to complex emissions scenarios which require solution at all grid points (Draxler and Hess 1998). Scenarios requiring the use of an Eulerian model include cases with contaminants sourced from

multiple locations or varying times. For this purpose, Eulerian methods require emissions to be defined on the same scale as the models computational grid.

On the other hand, Lagrangian models use a moving frame of reference, calculating the advection and diffusion equations independently from one another. This framework is favored when a pollutant can be traced back to a single-point source (Draxler and Hess 1998). This single-point source restricts the advection and dispersion calculations to be computed at only a few grid points; however this also means the Lagrangian models can define emissions at any resolution.

Hybrid Single-Particle Lagrangian Integrated Trajectory Model History

The Hybrid Single-Particle Lagrangian Integrated Trajectory (HYSPLIT) model is capable of computing simple parcel trajectories to more complex transport, dispersion, chemical transformation, or deposition simulations. In previous research endeavors, HYSPLIT was used to model atmospheric trajectories of pollutants including: radioactive material, wildfire smoke, wind-blown dust, allergens and volcanic ash (Stein et al. 2015).

HYSPLIT's lineage can be traced back to 1949 when the Special Project Section (SPS) of the U.S. Weather Bureau was charged with detecting radioactive debris originating from Soviet nuclear test sites. The SPS generated hand-calculated back trajectories following 500 hPa heights assuming a horizontal geostrophic flow. Assuming a steady state with homogeneous and stationary turbulence, air concentrations were estimated based on wind data collected from radiosonde balloon measurements twice daily (Stein et al. 2015). This work laid the foundation for ARL's trajectory and dispersion modeling capabilities.

In the late 1960s and early 1970s, ARL scientists developed the Mesoscale Diffusion Model in response to health and safety concerns at the Idaho National Reactor Testing Station (NRTS). The purpose of their work was to build upon their current transport and dispersion capabilities by incorporating changing weather conditions into planned or accidental releases of radioactive material into the atmosphere (Start & Wendell 1974). Scientists used a segmented Gaussian puff model using gridded data interpolated from a network of 21 tower-mounted wind sensors located within the boundaries of the NRTS to account for spatial variability of the horizontal wind flow near the surface. Their simulations incorporated time-varying diffusion rates in an attempt to model changing environments. Further advances in trajectory modeling occurred during the mid-1970s and 1980s when ARL researchers computed trajectories for concentrations of gaseous and particulate emissions using the Volcanic Ash Forecast and Dispersion (VAFTAD) Model (Heffter et al. 1993). Particles were modeled with an Eulerian advection technique using tri-linear interpolations of gridded horizontal wind components and vertical velocities. VAFTAD was expanded on previous trajectory approaches as it considered the deposition of falling particles from the ash cloud.

In the early 1980s, HYSPLIT version 1 was developed. In its initial version, segmented pollutants puffs were released near the surface and their trajectories followed for several days. This model differed from the previous experiment as it incorporated subdividing the daytime and nocturnal phase into separate trajectories to accurately depict the PBL. Transport was calculated solely from wind observations from rawinsonde data taken twice daily. The assumptions for these calculations included no vertical mixing over the planetary boundary layer (PBL) during the day while nocturnal wind

shear was modeled by vertically splitting the puffs that extended throughout the PBL into 300-m subpuffs (Draxler 1982). The second version of HYSPLIT interpolated rawinsonde and other observed data to estimate the vertical mixing coefficients that vary in space and time (Stein et al. 2015). HYSPLIT version 3 brought about the shift from using rawinsonde observations to utilizing gridded output from meteorological models. The model allowed for trajectory calculations to be completed using cylindrical puffs that grow with time and split when reaching the grid size of the meteorological data (Stein et al. 2015). Furthermore, HYSPLIT version 3 was the first version to incorporate chemistry into the model by introducing the chemical formation and deposition of sulfate.

HYSPLIT is currently on version 4 (HYSPLIT4). This version serves as the model used for this research. HYSPLIT4 takes a hybrid approach when calculating various components of a pollutant. It utilizes a Lagrangian approach (moving frame of reference) to calculate the advection, dispersion, and deposition of a pollutant. The model allows for the user to choose different Lagrangian approaches where the air masses being transported can be represented as three-dimensional particles, puffs or a hybrid of both (Stein et al. 2015). Moreover, HYSPLIT4 employs an Eulerian approach (stationary three-dimensional reference frame) to calculate the chemical transformations and pollutant concentrations.

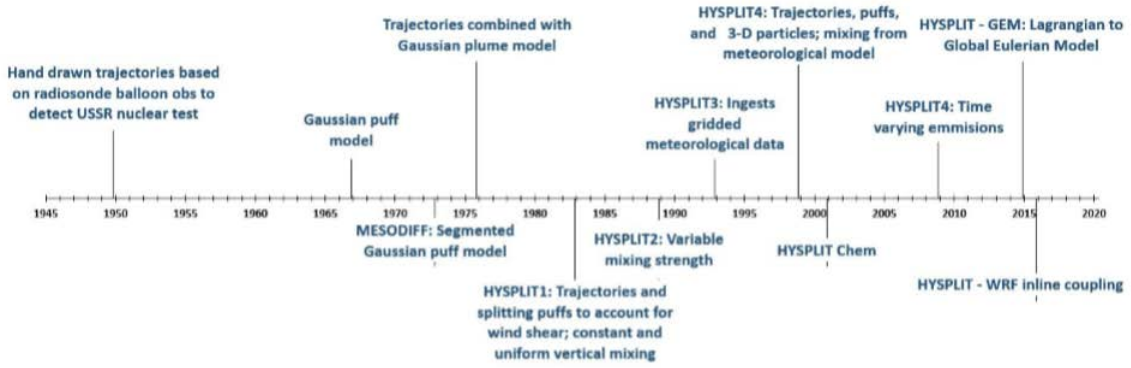

Figure 10: Timeline of HYSPLIT's development (Stein et al. 2015)

HYSPLIT Dynamics and Parameterizations

Parameterization is the process of emulating the effects of physical processes implicitly when they cannot be included explicitly by the governing equations or numerical methods (Warner 2011). Parameterization schemes are based on physical or statistical representations, but they both lead to error being introduced into the model. Physical parameterization error stems from the constraints of simulating a complex process into a simplified process. Statistical parameterizations error is when the model assumes a given process will occur in a certain percentage of cases when in actuality they may not. The following sections describe the model grids, parameterizations and calculations; all of which contribute a varying degree of error.

Meteorological Data Assimilation and Grids

HYSPLIT's grid is determined by the grid of the meteorological data passed into the model. Before these fields can be used by HSYPLIT some pre-processing must occur. Most meteorological models use some variation of a terrain following (σ) coordinate system; however, the data fields are usually interpolated to a variety of vertical coordinate systems prior to output (Draxler and Hess 1998). HYSPLIT is able to use a

variety of meteorological data sources as input; therefore, the profiles of the meteorological data at each horizontal grid points are linearly interpolated to a terrain following coordinate system,

$$\sigma = 1 - \frac{z}{z_{top}} \quad (1)$$

where z is the height relative to the terrain and z_{top} is the top of HYSPLIT's coordinate system (Draxler and Hess 1998). This conversion helps HYSPLIT maintain flexibility with data ingest. The model is capable of ingesting four different vertical coordinate systems: pressure-sigma, absolute-pressure, terrain-sigma, or a hybrid absolute-pressure sigma.

The dispersion model's horizontal grid system is determined by that of the meteorological input data (Draxler and Hess 1998). HYSPLIT supports three map projections: Polar Stereographic, Mercator, and Lambert Conformal. A simulation may contain multiple meteorological files, each with different grids and projections. For example, a simulation may start at a small, fine (regional) grid resolution to calculate precise concentration levels close to the source location and then switch to a larger, coarser (global) resolution further away to save on computational expense. This relationship is determined by:

$$U_{max}\Delta t < 0.75 \quad (2)$$

where U_{max} is the maximum transport velocity from the previous hour in grid-units per minute and Δt is the dynamic time step. HYSPLIT will choose either the meteorological data grid or the user-defined grid to complete all calculations, whichever one is finer, provided the product between U_{max} and Δt does not exceed 0.75.

HYSPLIT's flexibility to accomplish calculations on multiple model grids makes the model an ideal choice for transport and dispersion simulations. The downside in creating a model capable of ingesting various meteorological files is the plume forecast is only as accurate as the inputted meteorological data. Any error found in the weather forecast will be applied and propagated in HYSPLIT's forecast.

At a minimum, HYSPLIT requires the meteorological data ingested into the model to include the horizontal wind components (U and V), temperature (T), height (Z) or pressure (P), and the pressure at the surface (P_o). If wet deposition is included in the simulation, the meteorological model's rainfall field is required. Ground level winds ($\leq$ 10 m) are available in most meteorological models; however if these fields are not included HYSPLIT will estimate them using a logarithmic profile for neutral conditions (Draxler and Hess 1998).

Vertical Motion

Most meteorological models contain a vertical motion field relative to the model's native terrain following coordinate system. HSYPLIT uses this field to determine vertical velocity in its trajectory and dispersion calculations (Draxler and Hess 1998). If the vertical motion field is missing, or the desired simulation requires vertical motion to follow another surface, HYSPLIT has the option to replace this field. Vertical velocity (W_η) of a parcel on a selected surface(η) is computed from:

$$W_\eta = \frac{-\frac{\delta\eta}{\delta t} - u\frac{\delta\eta}{\delta x} - v\frac{\delta\eta}{\delta y}}{\frac{\delta\eta}{\delta z}} \quad (3)$$

given the slope of the surface and its local rate of change. The surface (η) can be defined as isobaric (p), isosigma (σ), isopynic (ρ), and isentropic (θ).

Transport & Advection Calculation

Once the horizontal and vertical components (U, V, and W_η) have been interpolated to the internal model grid, the advection equation is calculated. This equation is used to explicitly solve for the particle or puffs position as it travels across the grid. The advection of a particle or puff is computed from the average of the three-dimensional velocity vectors, V, at the particle's initial and first guess position (Draxler and Hess 1998). The velocity vectors are linearly interpolated in both space and time. The first guess position, $P'(t + \Delta t)$, is calculated by:

$$P'(t + \Delta t) = P(t) + V(P, t)\Delta t \quad (4)$$

where $P(t)$ is the particle's initial position, $V(P, t)$ is the velocity vector at the initial position and Δt is the time step. This first guess is used to calculate the final position.

$$P(t + \Delta t) = P(t) + \frac{1}{2}[V(P, t) + V(P', t + \Delta t)]\Delta t \quad (5)$$

where $V(P', t + \Delta t)$ is the velocity vector at the first guess position. The trajectory calculation is terminated if the particle or plume intersects the top of the model; however, the advection of the pollutant will continue along the ground it intersects the surface (Draxler and Hess 1998). The time step, Δt, can vary during the simulation. HYSPLIT will optimize the integration time step based on the grid size and maximum particle advection speed, but the advection distance per time step should be less than 0.75 of the meteorological grid spacing.

Dispersion Calculation

HYSPLIT can compute the air concentration either as a series of puffs with each containing a fraction of the overall mass of the pollutant or a release of many particles of the source of the simulation (Draxler and Hess 1998). This two-way approach is possible because HYSPLIT is a Lagrangian model. In the puff approach, the puff is advected according to the trajectory of its center position. The puff expands horizontally throughout time to account for the dispersive nature of the atmosphere. The puff will split when it exceeds the size of the grid space (Draxler and Hess 1998). Grid-scale processes are simulated by the puff-splitting process while sub-grid processes are modeled by the turbulent dispersion parameterization. The concentration of a specific grid space is thus the factional mass of the puff it contains. One downside to the puff approach is that it can create too many puffs, especially in the vertical direction, if the mixing is strong.

In the particle approach, the advection of the particle is determined by the random component of the motion of the atmosphere turbulence at that point in time. The air concentrations are calculated by adding the mass of all the particles in a grid cell. In the vertical dimension, it is advantageous to treat the pollutant as a particle in order to better capture the greater inhomogeneity of the vertical structure of the atmosphere (Draxler and Hess 1998). Ultimately, the most accurate representation of the dispersion of a pollutant is to treat it as a particle in the vertical direction and puff in the horizontal direction. Particles are more accurately represented in the vertical where discontinuities may be large. Puffs in the horizontal limit the number or particles required to adequately represent the horizontal distribution.

In both the particle and puff approaches the dispersion of the pollutant is parameterized by adding a turbulent component on to the mean velocity from the

meteorological data (Air Resource Laboratory 2018). The final position of the pollutant, P_{final}, in the particle approach after the turbulent component, V', is added to position that was calculated by the mean flow, P_{mean}, is:

$$P_{final}(t + \Delta t) = P_{mean}(t + \Delta t) + V'(t + \Delta t)\,\Delta t \quad (6)$$

The turbulent component is calculated from the previous time step's turbulent component, and auto-correlation coefficient, and Lagrangian time scale, T_{Li}:

$$V'(t + \Delta t) = R(\Delta t)V'(t) + V''(1 - R(\Delta t)^2)^{1/2} \quad (7)$$

where:

$$R(\Delta t) = \exp(\frac{-\Delta t}{T_{Li}}) \quad (8)$$

and V'' is the Gaussian random component which is derived from a computer-generated random number and the standard deviation of the velocity, σ_v.

The horizontal dispersion of a puff is parameterized by the puff growth rate when the puff's horizontal distribution standard deviation, σ_h, is smaller than the grid size. The standard deviation of the velocity defines the growth rate (Air Resources Laboratory 2018):

$$\sigma_V = \frac{d\sigma_h}{dt} \quad (9)$$

when the horizontal puff size is larger than the grid spacing, and thus must be split, the model resolves the dispersion explicitly (Draxler and Hess 1998). The method for splitting the puff depends on selection of a Top-Hat or Gaussian distributed puff. A Top-Hat distributed puff assumes a uniform concentration within 1.5 standard deviations (σ) of the center and zero outside. A Gaussian distributed puff assumes a normal distribution

of concentration about the center over 3σ (Air Resources Laboratory 2018). Figure 11 is a representation of a cross section of how the concentration of mass is about the axis.

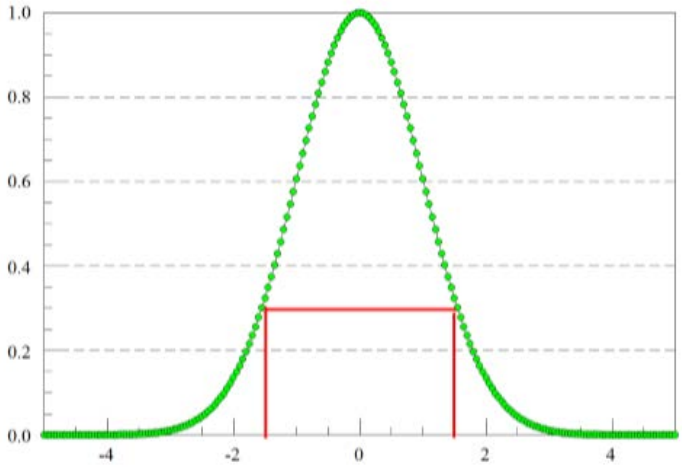

Figure 11: The concentration distribution about the axis of the mean trajectory for a Top-Hat (red) and Gaussian (green) puff. The horizontal axis is the number of σ while the vertical axis is the density function (Air Resource Laboratory 2018)

In the Top-Hat approach, the puff splits into four equal puffs of equal mass (25% of the original puff's mass). In the Gaussian approach, the puff splits into five new puffs with the center puff containing 60% of the original puff mass and the remaining four outside puffs each receive 10% of the original mass (Draxler and Hess 2018).

Concentration Calculation

The concentration calculation is dependent on whether the particle, Top-Hat puff, or Gaussian puff, is present within a grid cell. The single particle of mass, m, in a 3-D grid space concentration is determined by:

$$\Delta c = \frac{m}{\Delta x \Delta y \Delta z} \tag{10}$$

The incremental concentration by each Top-Hat puff of mass, m, to a grid point is defined by:

$$\Delta c = \frac{m}{(\pi r^2 \Delta z)} \tag{11}$$

where the horizontal radius (r) is $1.54\sigma_h$ and the vertical extent, Δz, is $3.08\sigma_z$ where σ_z is the standard deviation of the puff's vertical distribution (Draxler and Hess 2018). All grid nodes within the Top-Hat puff receive the same Δc. The incremental concentration contribution for a Gaussian puff is defined by:

$$\Delta c = \frac{m}{(2\pi {\sigma_h}^2 \Delta z)} \exp\left(\frac{-0.5x^2}{\sigma_h^2}\right) \tag{12}$$

where x is the distance from the puff's center to the grid-node and Δz is defined as the grid-cell height.

Mixing Layer Height

There are four main approaches utilized by HYSPLIT to estimate the mixing layer height. The default (and preferred way) is to use the mixing layer depth (Z_i) provided by the meteorological model. If the meteorological model does not include the required field, the second approach, the vertical temperature profile, will be used to estimate the height. It is assumed the mixing layer height is equal to height at which the potential temperature first exceeds the temperature of the ground by a value of 2K. The temperature profile is analyzed from the top down in an attempt to reduce the influence of shallow stable layers near the ground. In this approach, a minimum depth of 250 m is assumed for all hours because this level corresponds to the minimum height resolution of most meteorological input data. The downside of this approach is nighttime depths are overestimated for most geographic locations. The third approach to mapping the mixing layer is to calculate its depth from the turbulent kinetic energy (TKE) profile provided by the meteorological model. The depth is estimated to be the height at which the TKE

profile either decreases by a factor of two or falls below the threshold of 0.21. In this research, the inputted WRF model does not include the required fields to calculate the depth from the TKE profile; therefore the model defaults to calculating the height from the temperature profile. The final approach is to set a constant value for the depth of the boundary layer. It is important to note if a user desires to estimate Z_i either through the first or third approach, it is critical the meteorological model include the required fields, if not HYSPLIT will default to the second approach.

Boundary Layer Stability

There are two main approaches to estimate the boundary layer stability. The preferred method is to use the surface heat and momentum fluxes. When these fields are available from the inputted meteorological model, the friction velocity, u^*, is computed either from the scalar exchange coefficient, E.

$$u^* = \left(\frac{Eu}{\rho}\right)^{0.5} \tag{13}$$

where E is:

$$E = \rho C_D \tag{14}$$

where C_D is the drag coefficient and the product of E and u equivalent to stress due to that drag. The other option is compute the friction velocity directly from the vector momentum fluxes, F.

$$u^* = \left(\frac{|-F|}{\rho}\right)^{0.5} \tag{15}$$

The friction temperature in the boundary layer is computed from the sensible heat flux, H.

$$T^* = -\frac{H}{(\rho C_p u^*)} \quad (16)$$

where C_p is the heat constant (1005 J kg^{-1} K^{-1}) for dry air. Using these values the stability parameter for the planetary boundary layer can be defined as:

$$\frac{z}{L} = Z_2 k\, g\, T^* \left(u^{*2} T_2\right)^{-1} \quad (17)$$

where Z_2 indicated the height of the 2nd model level, which is assumed to be the depth of the surface layer.

When no fluxes are included in the meteorological model, a stability parameter is estimated from the wind (U) and temperature (T) profiles through the calculation of the bulk Richardson Number. This parameterization is labeled in the model as the "Boundary Layer Stability from the UT Profile." A meteorological sounding is used to compute the bulk Richardson Number, which is defined as:

$$R_b = g\, \Delta\theta\, \Delta z\, \{\theta_{12}[(\Delta U)^2 + (\Delta V)^2]\}^{-1} \quad (18)$$

where Δ indicates a gradient between levels one and two and θ_{12} is the layer averaged virtual potential temperature. From there, the friction velocity and friction temperature are then determined by:

$$u^* = k\, z_2\, \Delta U\, (\varphi_m \Delta z)^{-1} \quad (19)$$

$$T^* = k\, z_2\, \Delta\theta\, (\varphi_h \Delta z)^{-1} \quad (20)$$

where k is the von Karman's constant ($k \approx 0.4$) and the stability dependent normalized profiles (φ) for momentum (m) and heat (h) for a stable surface layer is $0 \leq \frac{z}{L} \leq 10$ (Beljaars and Holtslag 1991) and in an unstable surface layer is $-2 \leq \frac{z}{L} \leq 0$ (Kadar and Perepelkin 1989).

Horizontal and Vertical Turbulence

Before the horizontal and vertical turbulence and mixing can be determined, the boundary layer depth (Z_i) must be computed using one of the four approaches mentioned above in the boundary layer depth section. When the momentum and heat fluxes are available from the inputted meteorological data, the default approach to compute turbulence is from stability parameters. This approach uses the Kanthar-Clayson equations:

$$w'^2 = 3.0u^{*2}\left(1 - \frac{z}{Z_i}\right)^{\frac{3}{2}} \tag{21}$$

$$u'^2 = 4.0u^{*2}\left(1 - \frac{z}{Z_i}\right)^{\frac{3}{2}} \tag{22}$$

$$v'^2 = 4.5u^{*2}\left(1 - \frac{z}{Z_i}\right)^{\frac{3}{2}} \tag{23}$$

where the turbulent velocities are a function of the friction velocity, height and boundary layer depth. In this approach the horizontal and vertical components are explicitly predicted and are the default method of determining turbulence.

Turbulence can also be parameterized in terms of the vertical diffusivity for heat by:

$$K_z = k\, w_h\, z\, \left(1 - \frac{z}{Z_i}\right)^2 \tag{24}$$

where w_h (Equation 25) is the stability parameter and is a function of the friction velocity, Monin-Obukhov length, and convective velocity scale (w_*) (Troen and Mahrt 1986) and (Holtslag and Boville 1993).

$$w_h = f(u^*, \frac{1}{L}, w^*) \tag{25}$$

This parameterization is labeled in HYSPLIT as "Vertical Turbulence from Beljaars-Holtslag." In this approach the vertical diffusivity profile is converted to a turbulence value by:

$$\sigma_w = \left(\frac{K_h}{T_L}\right)^{0.5} \tag{26}$$

The horizontal turbulence components are assumed to be equal to the vertical component

$$w'^2 = u'^2 + v'^2 \tag{27}$$

The two approaches listed above are the defaults for determining the horizontal turbulence; however the horizontal turbulence can be replaced by a value computed from the deformation of the velocity field. This is accomplished by:

$$K_h = 2^{-0.5}(c\,X)^2 \left[\left(\left(\frac{\delta V}{\delta x}\right) + \left(\frac{\delta U}{\delta Y}\right) \right)^2 + \left(\left(\frac{\delta U}{\delta x}\right) - \left(\frac{\delta V}{\delta y}\right) \right)^2 \right]^{0.5} \tag{28}$$

where X is the meteorological grid size, and c = 0.14 (Smagorinsky 1963; Deardorff 1973).

If the turbulence is undefined by the user, HYSPLIT will select the optimum method (dependent on the fields available in the meteorological data) (ARL 2018). In this research, horizontal turbulence undefined will default to calculating the horizontal turbulence from the deformation of the velocity field.

Horizontal and Vertical Mixing

Similar to the horizontal turbulence approach above, the horizontal mixing coefficient (K_h) can be computed from the deformation velocity by:

$$K_h = 2^{-0.5}(c\ X)^2 \left[\left(\left(\frac{\delta V}{\delta x}\right) + \left(\frac{\delta U}{\delta Y}\right) \right)^2 + \left(\left(\frac{\delta U}{\delta x}\right) - \left(\frac{\delta V}{\delta y}\right) \right)^2 \right]^{0.5} \quad (29)$$

During convective conditions, vertical mixing through the inversion layer at $z = Z_i$ is computed based upon the surface flux parameters and the strength of the inversion by:

$$K_z = -C_s\ u^*\ T^* \left(\frac{\delta \theta}{\delta z}\right)^{-1} \quad (30)$$

where C_s = 0.4 (Beljaars and Betts 1993).

During stable conditions the vertical mixing is defined by the vertical diffusivity for heat using the mixing length theory by:

$$K_z = l^2 \left|\frac{\delta V}{\delta z}\right|\ \varphi_h \left(\frac{l}{L_o}\right)^{-1} \quad (31)$$

where l is the Blackadar-type mixing length proportional to height above ground and L_o is the local Obukhov length.

Near-field concentrations depend more on the individual details of the mixing profile while far field results depend more on the average mixing over the boundary layer. HYSPLIT is intended to be applied for long-range simulations; therefore there must be a unified approach to average the boundary layer mixing. This is accomplished by a single average value being determined for the boundary layer at each horizontal grid point. Each horizontal grid point will have a different value, all of which are combined together to map the boundary layer.

Deposition

Gases and aerosols have the potential to be removed from the pollutant plume through deposition (wet or dry) and radioactive decay (only if the pollutants are radioactive) (Draxler and Hess 1998). The total deposition in a plume is the summation of the removal constants. Dry deposition occurs when the plume intersects with the surface layer (advection of the pollutant will continue along the ground it intersects the surface). In HYSPLIT the surface layer is assumed to be to be second layer of the meteorological data. The removal constant is determined by:

$$\beta_{dry} = \frac{V_d}{\Delta Z_p} \tag{32}$$

where V_d is the deposition velocity and ΔZ_p is the depth of the pollutant layer (assumed to be the surface layer for dry removal. V_d is either defined as the gravitational settling velocity (defined by the user) or calculated by adding the resistances of the particles in the surface layer (Draxler and Hess 1998).

Wet deposition occurs when the plume interacts with cloudy air or when precipitation falls through the particles. Removal is computed using the scavenging ratio, S_r, for in-cloud processes (Draxler and Hess 1998). The in-cloud removal constant is determined by:

$$\beta_{inc} = \frac{F^t F_b S_r P_r}{\Delta Z_p} \tag{33}$$

where F^t is the faction of the pollutant layer that is below the cloud top, F_b is the fraction of the pollutant layer that is above the cloud base, and P_r is the precipitation rate (Draxler and Hess 1998). The scavenging coefficient for below cloud is represented by S_c. This coefficient is used to calculate the below cloud removal constant:

$$\beta_{bel} = S_c(1 - F_b) \quad (34)$$

The above equations describe wet deposition for particles; however wet deposition for gases is treated separately. Deposition of gases depends on the gas' solubility. For inert gases such as PMCH, used in CAPTEX, the deposition is a function of Henry's Law constant (H). H is a ration of the gas' equilibrium concentration in water to its concentration in air (Draxler and Hess 1998). The removal constant is determined from the surface to the top of the cloud layer and is defined as:

$$\beta_{gas} = \frac{F^t H\ R\ T\ P^r}{\Delta Z_p} \quad (35)$$

where R is the universal gas constant, and T is the temperature of the air (Draxler and Hess 1998). As mentioned previously, the total deposition of a plume is the summation of the removal constants. This is determined by:

$$D_{Total} = m\{1 - \exp[-\Delta t(\beta_{dry} + \beta_{inc} + \beta_{bel} + \beta_{gas})]\} \quad (36)$$

where m is the mass of the pollutant particle or puff.

Radioactive decay alone does not result in deposition; however deposited radioactive pollutants decay. The decay constant for radioactive matter, β_{rad}, is determined from its half- life,$T_{\frac{1}{2}}$, defined as:

$$\beta_{rad} = \frac{\ln(2)}{T_{\frac{1}{2}}} \quad (37)$$

and the radioactive decay of the pollutant's mass is determined by:

$$m_2 = m_1 \exp(-\beta_{rad}\Delta t) \quad (38)$$

III. Methodology

Chapter Overview

The purpose of this chapter is to describe the data in this research as well as the methodology for quantifying the spatial and temporal uncertainty in HYSPLIT's transport and dispersion simulations. This chapter describes how the datasets were obtained and created as well the methods of exposing the uncertainty within the sets.

CAPTEX Data

During CAPTEX2, 201 kg of PMCH was released from Dayton, OH between 1705 and 2005 on September 25, 1983. Over the next 68 hours the plume was detected and measured at 68 stations in the northeast United Sates and southeast Canada. The ARL compiled a file containing the 395 concentration measurements. This dataset was retrieved from ARL and served as the true measured data to be compared to the model's output. The measured CAPTEX file contains the time/date each sample was taken, the station ID number, the latitude and longitude of the observation, and the PMCH concentration level.

HYSPLIT CAPTEX Data

There are three overarching objectives in conducting an ensemble of the CAPTEX2 simulations. The first objective is to study the uncertainty in transport and dispersion modeling by testing the sensitivity of HYSPLIT on the resolution of the meteorology model ingested. To meet this goal the horizontal resolution of the meteorological model ingested into HYSPLIT, the WRF, will be run at a nested 3-km (coupled with 9-km), 9-km, and 27-km resolution. The WRF files were obtained from ARL. The second objective is to study the uncertainty in transport and dispersion

modeling by testing the sensitivity of HYPLIT on the resolution of concentration gird. For every meteorological model HYSPLIT's concentration gird will be set to a 1.0º x 1.0º and 0.25º x 0.25º. The last objective is to study the uncertainty associated with HYSPLIT's parameterization schemes. To accomplish this task thirty HYSPLIT parameterizations and initial conditions is tested for every meteorological model resolution and concentration grid. In total 198 model runs will be completed (see Table 2 for list of parameterizations and initial conditions).

Release Height	**Horizontal & Vertical Turbulence**	**Boundary Layer (BL) Stability & Mixing Layer (ML)**	**Vertical Motion**	**Other**
- 0m - 10m - 100m - 500m - 1000m - 2000m - 5000m	- Horizontal Turbulence From Variance - Horizontal Turbulence From Velocity Deformation - Horizontal Turbulence Undefined (defaulted to Velocity Deformation) - Vertical Turbulence From Beljaars-Holtslag - Vertical Turbulence From TKE Field - Vertical Turbulence From Variance - Vertical Turbulence From Kanthar-Clayson	- BL Stability from UT Profile - ML Constant at 1500m - ML From Temperature - ML From TKE Field - ML Remapped to BL Average	- Average Data - Constant Density - Damped Magnitude - From Divergence - Isentropic - Isobaric - Isosigma - Remapped From MSL to AGL	- Gaussian Puff - Gaussian Particle - Top Hat Puff - Top Hat Particle - Puff Growth Empirical - Dry Deposition

Table 2: List of parameterizations varied for each model simulation, organized by overarching model category. Each parameterization is run using both the 1.0º x 1.0º and 0.25º x 0.25º concentration gird coupled with the 3-km, 9-km or 27-km WRF. In total 198 model runs are completed.

This research builds upon on work conducted by Rolph et al. (2014) who modeled the dispersion, deposition, and decay of nuclear debris from six detonations at the Nevada Test site in the 1950s. Rolph et al. (2014) attempted to calculate the radioactive dose rates using HYSPLIT and compare these dose rate patterns to the six nuclear tests. Their goal was to use current research on nuclear source term to parameterize HYSPLIT so it can produce a realistic estimate of the magnitude and pattern of deposition. The six nuclear detonations in question are relatively small nuclear devices, with yields <50 kT (Rolph et al. 2014). It is assumed HSYPLIT would not be used to model the initial nuclear cloud growth, but instead simulate the cloud has stabilized before proceeding with the transport, dispersion and deposition of the plume (Rolph et al. 2014). Stabilization occurs after the temperature of the nuclear cloud is in equilibrium with the surrounding ambient air temperature. When this occurs entrainment of the surrounding outside air will end and the cloud will cease to grow vertically. Within the cloud nuclear particles have formed by three main processes: 1) directly by fission reaction, 2) by the condensation of vaporized material lofted from the surface, and 3) vaporized components of the device. The nuclear particles settle through the atmosphere at the particle's fall velocity. This velocity is based upon the size, shape and density of the particle. In this research, all particles are assumed to be spherical with a density of 2.5 g/cm^3.

To simulate the nuclear activity after cloud growth, the typical mushroom shape nuclear cloud is adapted using a technique called ARL Fallout Prediction Technique (AFPT). AFPT assumes the cloud is cylinder and divided into six layers from the surface to the top of the stabilized nuclear cloud (Figure 12). The thickness and height of every layer is dependent on the nuclear yield of the detonation and is determined by linearly

interpolating between the top and bottom cap (NATO 2010 Operations Manual) and between the surface and bottom of the cap. Figure 12 shows an example of the six layers of a 10-kT explosion. The layers range from 1700 m thick near the surface (non-shaded boxes) to 1000 m thick at the top of the cap (shaded boxes).

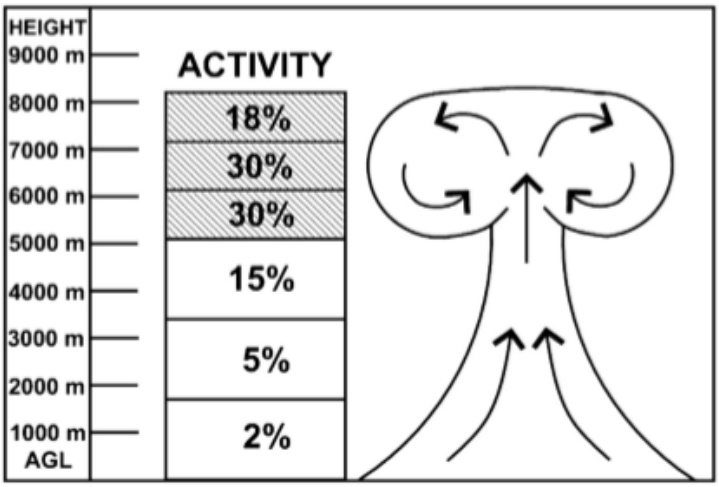

Figure 12: HYSPLIT representation of a nuclear mushroom cloud with the total activity fraction of the 10 kT explosion in each vertical segment (Hefffter 1969). The shaded layers define the cap of the nuclear cloud.

HYSPLIT Nuclear Cases Data

The main objective of Rolph et al. 2014 was to use current research on nuclear source term to parameterize HYSPLIT so it can produce a realistic estimate of the magnitude and pattern of deposition. Rolph et al. (2014) was successful in reproducing the general direction and deposition patterns of the six nuclear detonations listed above; therefore, their HYSPLIT set-up and configuration files were accessed through ARL and applied in this research. The set-up and configuration files were amended to test the sensitivity of the nuclear detonations on HYSPLIT's parameterization schemes. In total 150 simulations were completed (25 for each nuclear shot) (Table 3).

Horizontal & Vertical Turbulence	Boundary Layer (BL) Stability & Mixing Layer (ML)	Vertical Motion	Other
- Horizontal Turbulence From Variance - Horizontal Turbulence From Velocity Deformation - Horizontal Turbulence Undefined (defaulted to Velocity Deformation) - Vertical Turbulence From Beljaars-Holtslag - Vertical Turbulence From TKE Field - Vertical Turbulence From Variance - Vertical Turbulence From Kanthar-Clayson	- BL Stability from UT Profile - ML Constant at 1500m - ML From Temperature - ML From TKE Field - ML Remapped to BL Average	- Average Data - Constant Density - Damped Magnitude - From Divergence - Isentropic - Isobaric - Isosigma - Remapped From MSL to AGL	- Gaussian Puff - Gaussian Particle - Top Hat Puff - Top Hat Particle - Puff Growth Empirical

Table 3: List of parameterizations varied for each model simulation, organized by overarching model category. Each parameterization is run for the six nuclear detonations, Simon, Smoky, Sugar, Easy, Annie, and Harry. In total 150 simulations are completed

HYSPLIT was configured to simulate the transport and dispersion of the nuclear material for the six nuclear cases with yields ranging from 1.2 kT to 44 kT and stabilized cloud tops implied to reach between 3,700 m and 12,500 m AGL. The model was centered over the Nevada Test Site. After each HYSPLIT simulation is completed, the resulting deposition is converted to a dose rate with a fixed decay time of 12 hours

following detonation. The HYSPLIT predicted doses are compared to measured dose rates obtained from ARL.

HYSPLIT Statistics (CC, FB, FMS, KSP, Final Rank) Calculations

HYSPLIT calculates rank, a statistical parameter that evaluates and compare forecasted predicted concentration values to measured or observed concentration values. Rank encapsulates four statistical factors and renders a single value to compare forecasts with:- Correlation Coefficient (CC), Fractional Bias (FB), Figure of Merit in Space (FMS), and the Kolmogorov-Smirnov Parameter (KSP). These five values map are the key to quantifying the spatial accuracy of an each simulation.

Correlation Coefficient

The correlation coefficient is defined by:

$$CC = \sum \frac{(M_i - \bar{M})(P_i - \bar{P})}{\sqrt{\sum (M_i - \bar{M})^2 \sum (P_i - \bar{P})^2}} \tag{39}$$

where CC is the correlation coefficient, M_i is the individual data point measured concentration, $\bar{M}$ is the average measured concentration, P_i is the individual data point model predicted concentration, $\bar{P}$ is the average model predicted concentration. This factor ranges in value from negative one to positive one where zero indicates no correlation and + (-) indicates a positive (negative) linear relationship between the two data sets.

Fractional Bias

The fractional bias is defined by:

$$FB = 2\frac{(\bar{P} - \bar{M})}{(\bar{P} + \bar{M})} \tag{40}$$

where FB is the fractional bias. Fractional bias values range from negative two to positive two where zero indicated no bias. Negative values indicate an under prediction of concentrations and positive values indicate an over prediction of concentrations.

Figure of Merit in Space

The figure of merit in space is defined by:

$$FMS = 100\frac{(N_p \cap N_m)}{(N_p \cup N_m)} \tag{41}$$

where FMS is the figure of merit in space, N_p is the number of samplers with a model predicted concentration greater than zero, N_m is the number of samplers with measured concentration greater than zero, $N_p \cap N_m$ is the intersection of samplers with positive model predicted and measured concentration values, and $N_p \cup N_m$ is the union of all samplers with positive concentration values. Values are a percentage and indicate the degree of overlap between the measured and predicted pollutant clouds. Higher percentages are desired, as this indicates the model forecast matched well with measured concentrations.

Kolmogorov-Smirnov Parameter

The Kolmogorov-Smirnov parameter is defined by:

$$KSP = Max|D(M_k) - D(P_k)| \tag{42}$$

where KSP is the Kolmogorov-Smirnov parameter, $D(M_k)$ is the cumulative distribution of the measured concentrations across a range of values k, and $D(P_k)$ is the cumulative distribution of the model predicted concentrations across a range of values k. The KSP identifies and quantifies the maximum difference between the two cumulative distributions and is a measure of how well the model reproduces the measured

concentration distribution. It is represented as a percentage, with lower percentages indicating high quality forecasts, or more similar cumulative distribution between the predicted and measured concentration values.

Final Rank

The final rank is defined by:

$$Rank = CC^2 + \ 1 - \ \left|\frac{FB}{2}\right| + \frac{FMS}{100} + \ (1 - \frac{KSP}{100}) \tag{43}$$

where rank is the normalized sum of the four statistical factors described above. Each statistical factor is given equal weight, where a value of one in each term represents an ideal forecast. Final rank values ranges from zero (worst) to four (best). Rank encompasses the correlation between the measured and predicted data, any bias in concentration forecast, how well the measured and predicted pollutant areas match up and the maximum difference between the cumulative distributions.

The built-in model utility is used to calculate these statistics, however before the ensemble varying the parameterizations is conducted each calculation is verified using MATLAB. Using CAPTEX measured data, the control case from the 3-km, 9-km, and 27-km WRF using a one degree and quarter degree concentration grid simulation is accomplished. The five statistics are computed using the measured and predicted datasets. Table 4 and 5 show no significant discrepancies between the model calculated and MATLAB calculated statistics; therefore, it is concluded the statistical output from HYSPLIT can be used with confidence.

	FB	CC	FMS	KSP	Rank
WRF3-KM-HYSPLIT	-0.15	0.64	72.47	7	2.98
WRF3-KM-MATLAB	-0.149	0.647	72.44	7	2.97
WRF9-KM-HYSPLIT	-0.16	0.66	70.73	6	3.01
WRF9-KM-MATLAB	-0.157	0.66	70.91	6	3.02
WRF27-KM-HYSPLIT	-0.31	0.65	70.71	9	2.98
WRF27-KM-MATLAB	-0.303	0.654	70.95	9	2.97

Table 4: Comparison of Fractional Bias (FB), Correlation Coefficient (CC), Figure of Merit in Space (FMS), Kolmogorov-Smirnov Parameter (KSP), and Final Rank computed for the CAPTEX2 control case from HYSPLIT and MATLAB. Each run was completed using a 0.25 º x 0.25º concentration grid.

	FB	CC	FMS	KSP	Rank
WRF3-KM-HYSPLIT	-0.43	0.69	57.83	12	2.72
WRF3-KM-MATLAB	-0.441	0.688	57.80	12	2.71
WRF9-KM-HSYPLIT	-0.42	0.70	58.36	14	2.72
WRF9-KM-MATLAB	-0.425	0.694	58.33	14	2.72
WRF27-KM-HYSPLIT	-0.55	0.65	60.12	10	2.65
WRF27-KM-MATLAB	-0.55	0.647	60.0	10	2.65

Table 5: Comparison of Fractional Bias (FB), Correlation Coefficient (CC), Figure of Merit in Space (FMS), Kolmogorov-Smirnov Parameter (KSP), and Final Rank computed for the CAPTEX2 control case from HYSPLIT and MATLAB. Each run was completed using a 1.0º x 1.0º concentration grid.

Timing Error Calculations

Uncertainty in atmospheric transport and dispersions models is not only a measure of how accurate the model depicts the location of a pollutant in the x-y-z sphere (described by the five statistical values above), but must also include the timing a

pollutant was first observed at that location. To accomplish this, MATLAB was utilized to separate the CAPTEX measured data and HSYPLIT output data into individual .txt files organized by station identifier and the parameterization being tested. The calculation seen in Equation 44 is applied to every station.

$$|Onset\ Time_{CAPTEX} - \ Onset\ Time_{HYSPLIT}| \tag{44}$$

The time stamp when PMCH was first detected at each station during CAPTEX (measured data) was compared to the time stamp when PMCH was calculated at each station by HYSPLIT (predicted data). This data describes which parameterization (boundary layer stability, turbulence scheme, release height, etc), meteorological model resolution, and concentration grid best determines the onset timing at each station with the measured data.

IV. Analysis and Results

Chapter Overview:

The purpose of this chapter is to evaluate and convey the results from the atmospheric transport and dispersion uncertainty studies. These results include the statistical and timing error results from CAPTEX2 as well as the statistical results from the stabilized nuclear fallout cases. Lastly, this chapter will communicate the success rate of HYSPLIT in the CAPTEX2 simulations.

CAPTEX Statistical Results

The five statistical rankings: Fractional Bias (FB), Correlation Coefficient (CC), Figure of Merit in Space (FMS), Kolmogorov-Smirnov Parameter (KSP), and Final Rank was computed by HYSPLIT for the 198 model runs. HYSPLIT's statistics for the 0.25º x 0.25º concentration grid can be seen in Tables 6 (3-km), 7 (9-km) and 8 (27-km) while the statistics for the 1.0º x 1.0º concentration grid are displayed in Tables 9 (3-km), 10 (9-km), and 11 (27-km).

WRF-3km 0.25 x 0.25 Deg Concentration Grid	Fractional Bias	Correlation Coefficient	Figure of Merit in Space	Kolmogorov-Smirnov Parameter	Final Rank
Control Case	-0.15	0.64	72.47	7	2.98
Isobaric	-0.58	0.61	71.02	9	2.70
Isentropic	-0.60	0.58	74.67	15	2.64
Constant Density	-0.95	0.53	68.44	12	2.37
Isosigma	-0.43	0.59	70.33	9	2.75
From Divergence	-0.17	0.62	69.92	9	2.9
Remap MSL to AGL	-0.37	0.64	71.49	10	2.84
Vertical From Average Data	-0.15	0.64	72.47	7	2.98
Damped Magnitude	-0.15	0.64	72.47	7	2.98
Vertical Turbulence - Beljaars-Holtslag	0.57	0.62	69.58	10	2.70

Vertical Turbulence - Kanthar-Clayson	-0.15	0.64	72.47	7	2.98
Vertical Turbulence - TKE Field	-0.15	0.64	72.47	7	2.98
Vertical Turbulence - Variance	-0.15	0.64	72.47	7	2.98
Horizontal Turbulence - Velocity Deformation	0.00	0.42	72.03	11	2.78
Horizontal Turbulence - Undefined – Defaulted to Velocity Deformation	0.00	0.42	72.03	11	2.78
Horizontal Turbulence - Variance	-0.15	0.64	72.47	7	2.98
BL Stability from U/T profile	-0.45	0.81	70.70	10	3.03
Vertical Mixing replaced by PBL average	-0.29	0.54	70.33	9	2.76
Mixed Layer from temp profile	-0.11	0.65	70.56	8	2.99
Mixed Layer from TKE profile	-0.11	0.65	70.56	8	2.99
Mixed Layer Constant at 1500m Min at 250	-0.24	0.57	69.96	11	2.8
Puff Growth Empirical	-0.15	0.64	72.47	7	2.98
Release 0m	-0.15	0.64	71.77	8	2.97
Release 100m	-0.15	0.63	71.66	7	2.97
Release 500m	-0.17	0.63	71.95	8	2.95
Release 1000m	-0.20	0.62	71.95	7	2.93
Release 2000m	-1.59	0.49	70.39	21	1.94
Release 5000m	-2.0	0.0	0.0	100	0.0
Wet Deposition	Could not complete because meteorological data does not have precipitation field required to complete calculations.				
Dry Deposition	-0.75	0.54	72.47	13	2.51
Wet & Dry Deposition	Could not complete because meteorological data does not have precipitation field required to complete calculations.				
Gaussian-Horizontal, Top Hat Vertical Puff	0.03	0.3	62.98	14	2.57
Top Hat Horizontal & Vertical Puff	-0.03	0.29	66.94	13	2.6
Gaussian-Horizontal, Particle Vertical	0.02	0.43	63.73	7	2.75
Top Hat Horizontal, Particle Vertical	0.01	0.41	67.55	9	2.75

Table 6: Fractional Bias (FB), Correlation Coefficient (CC), Figure of Merit in Space (FMS), Kolmogorov-Smirnov Parameter (KSP), and Final Rank computed for the CAPTEX2 from HYSPLIT using the WRF 3-km and 0.25º x 0.25º concentration grid. The red blocks indicate the lowest scoring statistic in that column while the green blocks indicate the highest scoring statistic in that column.

WRF-9km 0.25 x 0.25 Deg Concentration Grid	Fractional Bias	Correlation Coefficient	Figure of Merit in Space	Kolmogorov-Smirnov Parameter	Final Rank
Control Case	-0.16	0.66	70.73	6	3.01
Isobaric	-0.52	0.57	69.55	9	2.67
Isentropic	-0.39	0.60	72.25	16	2.72
Constant Density	-0.93	0.51	67.76	10	2.37
Isosigma	-0.37	0.58	69.68	7	2.78
From Divergence	-0.18	0.65	72.08	9	2.96
Remap MSL to AGL	-0.49	0.69	70.56	12	2.81
Vertical From Average Data	-0.21	0.66	71.43	7	2.98
Damped Magnitude	-0.30	0.64	71.26	6	2.92
Vertical Turbulence - Beljaars-Holtslag	0.55	0.58	71.01	10	2.67
Vertical Turbulence - Kanthar-Clayson	-0.16	0.66	70.92	6	3.01
Vertical Turbulence - TKE Field	-0.13	0.63	70.68	6	2.99
Vertical Turbulence - Variance	-0.16	0.66	70.00	6	3.00
Horizontal Turbulence - Velocity Deformation	-0.07	0.41	70.46	11	2.72
Horizontal Turbulence - Undefined – Defaulted to Velocity Deformation	-0.07	0.41	70.46	11	2.72
Horizontal Turbulence - Variance	-0.16	0.66	70.00	6	3.00
BL Stability from U/T profile	-0.17	0.79	68.97	3	3.19
Vertical Mixing replaced by PBL average	-0.30	0.55	73.44	8	2.81
Mixed Layer from temp profile	-0.12	0.63	71.95	7	2.99
Mixed Layer from TKE profile	-0.12	0.63	71.95	7	2.99
Mixed Layer Constant at 1500m Min at 250	-0.31	0.55	71.43	9	2.78
Puff Growth Empirical	-0.16	0.66	70.00	6	3.00
Release 0m	-0.16	0.66	70.92	6	3.01
Release 100m	-0.15	0.67	70.85	7	3.01
Release 500m	-0.18	0.66	70.59	7	2.98

Release 1000m	-0.19	0.63	70.16	6	2.95
Release 2000m	-1.25	0.51	70.64	15	2.20
Release 5000m	-2.00	0.00	0.00	100	0.00
Wet Deposition	Could not complete because meteorological data does not have precipitation field required to complete calculations.				
Dry Deposition	-0.70	0.57	70.73	10	2.58
Wet & Dry Deposition	Could not complete because meteorological data does not have precipitation field required to complete calculations.				
Gaussian-Horizontal, Top Hat Vertical Puff	-0.17	0.28	64.73	15	2.49
Top Hat Horizontal & Vertical Puff	-0.06	0.24	64.73	14	2.53
Gaussian-Horizontal, Particle Vertical	-0.13	0.42	63	6	2.68
Top Hat Horizontal, Particle Vertical	-0.16	0.51	68.85	5	2.82

Table 7: Fractional Bias (FB), Correlation Coefficient (CC), Figure of Merit in Space (FMS), Kolmogorov-Smirnov Parameter (KSP), and Final Rank computed for the CAPTEX2 from HYSPLIT using the WRF 9-km and 0.25º x 0.25º concentration grid. The red blocks indicate the lowest scoring statistic in that column while the green blocks indicate the highest scoring statistic in that column.

WRF-27km 0.25 x 0.25 Deg Concentration Grid	Fractional Bias	Correlation Coefficient	Figure of Merit in Space	Kolmogorov-Smirnov Parameter	Final Rank
Control Case	-0.31	0.65	70.71	9	2.98
Isobaric	-0.49	0.60	69.62	12	2.69
Isentropic	-0.44	0.62	70.98	18	2.69
Constant Density	-0.89	0.55	69.53	13	2.42
Isosigma	-0.40	0.62	70.17	10	2.79
From Divergence	-0.69	0.63	72.29	11	2.67
Remap MSL to AGL	-0.52	0.66	69.29	11	2.76
Vertical From Average Data	-0.31	0.65	70.71	9	2.98
Damped Magnitude	-0.31	0.65	70.71	9	2.98
Vertical Turbulence - Beljaars-Holtslag	0.28	0.64	67.53	12	2.82
Vertical Turbulence - Kanthar-Clayson	-0.31	0.65	70.95	9	2.98
Vertical Turbulence - TKE Field	-0.31	0.65	70.95	9	2.98
Vertical Turbulence - Variance	-0.31	0.65	70.95	9	2.98

Horizontal Turbulence - Velocity Deformation	-0.22	0.43	68.83	14	2.63
Horizontal Turbulence - Undefined – Defaulted to Velocity Deformation	-0.22	0.43	68.83	14	2.63
Horizontal Turbulence - Variance	-0.31	0.65	70.95	9	2.98
BL Stability from U/T profile	-0.47	0.73	66.23	16	2.80
Vertical Mixing replaced by PBL average	-0.42	0.54	71.37	10	2.70
Mixed Layer from temp profile	-0.26	0.65	69.26	9	2.90
Mixed Layer from TKE profile	-0.26	0.65	69.26	9	2.90
Mixed Layer Constant at 1500m Min at 250	-0.46	0.57	67.09	14	2.63
Puff Growth Empirical	-0.31	0.65	70.95	9	2.98
Release 0m	-0.32	0.66	71.25	9	2.90
Release 100m	-0.31	0.65	71.01	9	2.90
Release 500m	-0.32	0.64	71.13	9	2.88
Release 1000m	-0.35	0.63	68.57	9	2.82
Release 2000m	-1.16	0.47	69.13	15	2.18
Release 5000m	-2.00	0.00	0.00	100	0.00
Wet Deposition	Could not complete because meteorological data does not have precipitation field required to complete calculations.				
Dry Deposition	-0.76	0.55	70.71	14	2.49
Wet & Dry Deposition	Could not complete because meteorological data does not have precipitation field required to complete calculations.				
Gaussian-Horizontal, Top Hat Vertical Puff	-0.52	0.43	64.39	14	2.43
Top Hat Horizontal & Vertical Puff	-0.34	0.40	63.64	16	2.47
Gaussian-Horizontal, Particle Vertical	-0.36	0.58	63.01	6	2.73
Top Hat Horizontal, Particle Vertical	-0.32	0.56	70.63	10	2.75

Table 8: Fractional Bias (FB), Correlation Coefficient (CC), Figure of Merit in Space (FMS), Kolmogorov-Smirnov Parameter (KSP), and Final Rank computed for the CAPTEX2 from HYSPLIT using the WRF 27-km and 0.25º x 0.25º concentration grid. The red blocks indicate the lowest scoring statistic in that column while the green blocks indicate the highest scoring statistic in that column.

WRF-3km 1.0 x 1.0 Deg Concentration Grid	Fractional Bias	Correlation Coefficient	Figure of Merit in Space	Kolmogorov-Smirnov Parameter	Final Rank
Control Case	-0.43	0.69	57.83	12	2.72
Isobaric	-0.73	0.66	58.95	7	2.59
Isentropic	-0.72	0.53	60.32	6	2.47
Constant Density	-0.99	0.51	59.19	7	2.29
Isosigma	-0.65	0.69	57.75	9	2.64
From Divergence	-0.39	0.66	59.38	11	2.73
Remap MSL to AGL	-0.56	0.67	58.54	9	2.66
Vertical From Average Data	-0.43	0.69	57.83	12	2.72
Damped Magnitude	-0.43	0.69	57.83	12	2.72
Vertical Turbulence - Beljaars-Holtslag	0.15	0.75	59.81	13	2.96
Vertical Turbulence - Kanthar-Clayson	-0.43	0.69	57.83	12	2.72
Vertical Turbulence - TKE Field	-0.43	0.69	57.83	12	2.72
Vertical Turbulence - Variance	-0.43	0.69	57.83	12	2.72
Horizontal Turbulence - Velocity Deformation	-0.35	0.69	60.83	11	2.79
Horizontal Turbulence - Undefined – Defaulted to Velocity Deformation	-0.35	0.69	60.83	11	2.79
Horizontal Turbulence - Variance	-0.43	0.69	57.83	12	2.72
BL Stability from U/T profile	-0.79	0.78	56.52	7	2.71
Vertical Mixing replaced by PBL average	-0.50	0.61	58.46	10	2.60
Mixed Layer from temp profile	-0.38	0.69	58.01	11	2.76
Mixed Layer from TKE profile	-0.38	0.69	58.01	11	2.76
Mixed Layer Constant at 1500m Min at 250	-0.48	0.65	59.87	7	2.71
Puff Growth Empirical	-0.43	0.69	57.83	12	2.72
Release 0m	-0.42	0.69	58.72	12	2.73

Release 100m	-0.41	0.69	57.88	12	2.73
Release 500m	-0.45	0.69	58.01	11	2.72
Release 1000m	-0.47	0.68	57.78	12	2.68
Release 2000m	-1.63	0.56	60.44	23	1.88
Release 5000m	-2.00	0.00	0.00	100	0.00
Wet Deposition	Could not complete because meteorological data does not have precipitation field required to complete calculations.				
Dry Deposition	-0.94	0.61	57.83	7	2.41
Wet & Dry Deposition	Could not complete because meteorological data does not have precipitation field required to complete calculations.				
Gaussian-Horizontal, Top Hat Vertical Puff	0	0.16	61.02	9	2.55
Top Hat Horizontal & Vertical Puff	-0.08	0.13	64.84	8	2.55
Gaussian-Horizontal, Particle Vertical	-0.53	0.15	57.58	8	2.26
Top Hat Horizontal, Particle Vertical	-0.50	0.11	62.37	8	2.31

Table 9: Fractional Bias (FB), Correlation Coefficient (CC), Figure of Merit in Space (FMS), Kolmogorov-Smirnov Parameter (KSP), and Final Rank computed for the CAPTEX2 from HYSPLIT using the WRF 3-km and 1.0º x 1.0º concentration grid. The red blocks indicate the lowest scoring statistic in that column while the green blocks indicate the highest scoring statistic in that column.

WRF-9km 1.0 x 1.0 Deg Concentration Grid	Fractional Bias	Correlation Coefficient	Figure of Merit in Space	Kolmogorov-Smirnov Parameter	Final Rank
Control Case	-0.42	0.70	58.36	14	2.72
Isobaric	-0.67	0.67	59.08	8	2.62
Isentropic	-0.60	0.56	59.37	6	2.55
Constant Density	-0.97	0.52	59.06	7	2.31
Isosigma	-0.60	0.69	57.70	10	2.65
From Divergence	-0.43	0.70	59.69	12	2.75
Remap MSL to AGL	-0.73	0.72	59.02	6	2.68
Vertical From Average Data	-0.45	0.68	57.88	13	2.69
Damped Magnitude	-0.55	0.70	58.36	12	2.68
Vertical Turbulence - Beljaars-Holtslag	0.18	0.71	60.13	14	2.88
Vertical Turbulence - Kanthar-Clayson	-0.42	0.70	60.13	14	2.72

Vertical Turbulence - TKE Field	-0.42	0.70	58.36	14	2.72
Vertical Turbulence - Variance	-0.42	0.70	58.36	14	2.72
Horizontal Turbulence - Velocity Deformation	-0.35	0.66	59.94	13	2.74
Horizontal Turbulence - Undefined – Defaulted to Velocity Deformation	-0.35	0.66	59.94	13	2.74
Horizontal Turbulence -Variance	-0.42	0.70	58.36	14	2.72
BL Stability from U/T profile	-0.44	0.71	57.69	17	2.69
Vertical Mixing replaced by PBL average	-0.49	0.60	59.08	11	2.59
Mixed Layer from temp profile	-0.38	0.68	58.66	13	2.72
Mixed Layer from TKE profile	-0.38	0.68	58.66	13	2.72
Mixed Layer Constant at 1500m Min at 250	-0.54	0.65	59.56	7	2.68
Puff Growth Empirical	-0.42	0.70	58.36	14	2.72
Release 0m	-0.41	0.70	58.43	14	2.72
Release 100m	-0.41	0.69	58.08	13	2.73
Release 500m	-0.43	0.69	58.08	13	2.71
Release 1000m	-0.44	0.68	58.79	13	2.69
Release 2000m	-1.35	0.63	60.62	15	2.17
Release 5000m	-2	0	0	100	0
Wet Deposition	Could not complete because meteorological data does not have precipitation field required to complete calculations.				
Dry Deposition	-0.87	0.61	58.36	6	2.46
Wet & Dry Deposition	Could not complete because meteorological data does not have precipitation field required to complete calculations.				
Gaussian-Horizontal, Top Hat Vertical Puff	-0.16	0.08	62.07	5	2.50
Top Hat Horizontal & Vertical Puff	-0.13	0.09	65.31	7	2.53
Gaussian-Horizontal, Particle Vertical	-0.43	0.11	57.88	10	2.28
Top Hat Horizontal, Particle Vertical	-0.46	0.20	62.50	11	2.32

Table 10: Fractional Bias (FB), Correlation Coefficient (CC), Figure of Merit in Space (FMS), Kolmogorov-Smirnov Parameter (KSP), and Final Rank computed for the CAPTEX2 from HYSPLIT using the WRF 9-km and 1.0^{0} x 1.0^{0} concentration grid. The red blocks indicate the lowest scoring statistic in that column while the green blocks indicate the highest scoring statistic in that column.

WRF-27km 1.0 x 1.0 Deg Concentration Grid	Fractional Bias	Correlation Coefficient	Figure of Merit in Space	Kolmogorov-Smirnov Parameter	Final Rank
Control Case	-0.55	0.65	60.12	10	2.65
Isobaric	-0.69	0.67	60.51	5	2.66
Isentropic	-0.65	0.49	61.26	9	2.44
Constant Density	-0.97	0.53	60.38	7	2.32
Isosigma	-0.66	0.70	59.87	7	2.68
From Divergence	-0.86	0.65	60.57	8	2.52
Remap MSL to AGL	-0.74	0.66	58.77	7	2.58
Vertical From Average Data	-0.55	0.65	60.12	10	2.65
Damped Magnitude	-0.55	0.65	60.12	10	2.65
Vertical Turbulence - Beljaars-Holtslag	-0.06	0.69	60.39	13	2.93
Vertical Turbulence - Kanthar-Clayson	-0.55	0.65	60.12	10	2.65
Vertical Turbulence - TKE Field	-0.55	0.65	60.12	10	2.65
Vertical Turbulence - Variance	-0.55	0.65	60.12	10	2.65
Horizontal Turbulence - Velocity Deformation	-0.51	0.64	60.59	10	2.67
Horizontal Turbulence - Undefined – Defaulted to Velocity Deformation	-0.51	0.64	60.59	10	2.67
Horizontal Turbulence -Variance	-0.55	0.65	60.12	10	2.65
BL Stability from U/T profile	-0.91	0.61	60.00	9	2.43
Vertical Mixing replaced by PBL average	-0.61	0.56	59.44	10	2.51
Mixed Layer from temp profile	-0.51	0.64	59.44	11	2.64

Mixed Layer from TKE profile	-0.51	0.64	59.44	11	2.64
Mixed Layer Constant at 1500m Min at 250	-0.65	0.61	61.22	6	2.6
Puff Growth Empirical	-0.55	0.65	60.12	10	2.65
Release 0m	-0.55	0.65	59.02	10	2.64
Release 100m	-0.55	0.65	59.57	10	2.64
Release 500m	-0.56	0.64	58.72	10	2.62
Release 1000m	-0.58	0.63	59.08	10	2.6
Release 2000m	-1.3	0.55	61.11	14	2.13
Release 5000m	-2.00	0.00	0.00	100	0
Wet Deposition	Could not complete because meteorological data does not have precipitation field required to complete calculations.				
Dry Deposition	-0.92	0.56	60.12	6	2.4
Wet & Dry Deposition	Could not complete because meteorological data does not have precipitation field required to complete calculations.				
Gaussian-Horizontal, Top Hat Vertical Puff	-0.55	0.26	62.63	5	2.37
Top Hat Horizontal & Vertical Puff	-0.43	0.27	64.07	6	2.44
Gaussian-Horizontal, Particle Vertical	-0.59	0.41	59.19	8	2.38
Top Hat Horizontal, Particle Vertical	-0.60	0.29	63.76	7	2.35

Table 11: Fractional Bias (FB), Correlation Coefficient (CC), Figure of Merit in Space (FMS), Kolmogorov-Smirnov Parameter (KSP), and Final Rank computed for the CAPTEX2 from HYSPLIT using the WRF 27-km and 1.0º x 1.0º concentration grid. The red blocks indicate the lowest scoring statistic in that column while the green blocks indicate the highest scoring statistic in that column.

The parameterizations included in the meteorological model and the parameterizations prescribed in HYSPLIT are a significant source of error. In Tables 6-11, the green highlighted boxes coincide with the highest performing parameterizations, while the red boxes align with the lowest performing parameterizations. In the CAPTEX2 control case, the tracer was released from 10m above ground, the vertical motion and boundary layer stability was determined from the inputted WRF model, all remaining parameters (i.e. turbulence, mixing layer etc.) were set to the model's defaults (see background section for default configurations). Across all runs the simulations with the

following parameterizations performed well include: mapping the boundary layer from the UT profile, determining vertical turbulence using either the Kanthar-Clayson approach or Beljaars-Holtslag approach, and mapping the mixed layer from the temperature profile.

Of the six sets of runs, the highest ranking model configuration was using a 0.25º x 0.25º concentration grid coupled with the 9-km WRF, approximating the boundary layer conditions from the UT profile (Rank: 3.19). Stability from profiles, such as that from the UT profile, are instantaneous values that are valid at the model's time step (Air Resource Laboratory 2018). On the other hand, stabilities derived from flux, such as that from the YSU scheme in the WRF model, are based upon time-averaged heat and momentum fluxes. The YSU scheme is a non-local scheme; meaning that communication between PBL layers is unrestricted. This means each layer communicates the physical states each other. Each layer to know the state the physical states of all of the other layers. This allows deeper mixing of energy from the free atmosphere above the PBL into the layers within the PBL, resulting in a more realistic daytime PBL height when compared to local PBL schemes (Cohen et al. 2015).

These results are consistent with the work on source term estimation of atmospheric pollutants. The planetary boundary layer schemes in meteorological models utilized in HYSPLIT simulations significantly impacts the source term estimation outcome (Zoellick 2019). Representing the planetary boundary layer accurately is crucial in long range transport and dispersion releases such as CAPTEX. Most of the dispersion of the CAPTEX plume occurs in the planetary boundary layer. Although the boundary layer stability from the UT profile proved to be the most fruitful parameterization in this

research, there is no single right answer that applies to all cases. The stability profile chosen depends upon the frequency of the meteorological data, the time duration of the flux integral and meteorological conditions (Air Resource Laboratory 2018).

Excluding releases of the pollutant from heights other than at the surface, the lowest ranking model configuration was using 1) a 1.0º x 1.0º concentration grid with the 3-km WRF coupled with a Top-Hat concentration distribution with the emission treated as a series of particles (Rank: 2.31) and 2) the a 1.0º x 1.0º concentration grid with the 3-km WRF coupled with the vertical motion parameterized using a constant density field (Rank: 2.31). The Top-Hat concentration distribution with the emission treated as a series of particle, fails to more accurately capture the expansion of the pollutant plume due to the dispersive nature of the atmosphere compared to model default approach. The default approach uses particle dispersion in the vertical direction and puff dispersion in the horizontal (Draxler 1998). This allows for particles to be used in the vertical, where discontinuities may be large, and puffs in the horizontal (and subsequently puff-splitting) to limit the number of particles that are required to adequately represent the horizontal distribution (Draxler 1998). Displays of the concentration plume for the control case (using the 9-km WRF on a 0.25º x 0.25º concentration grid), boundary layer stability from UT profile parameterization, and constant density parameterization are seen in Figures 13-15.

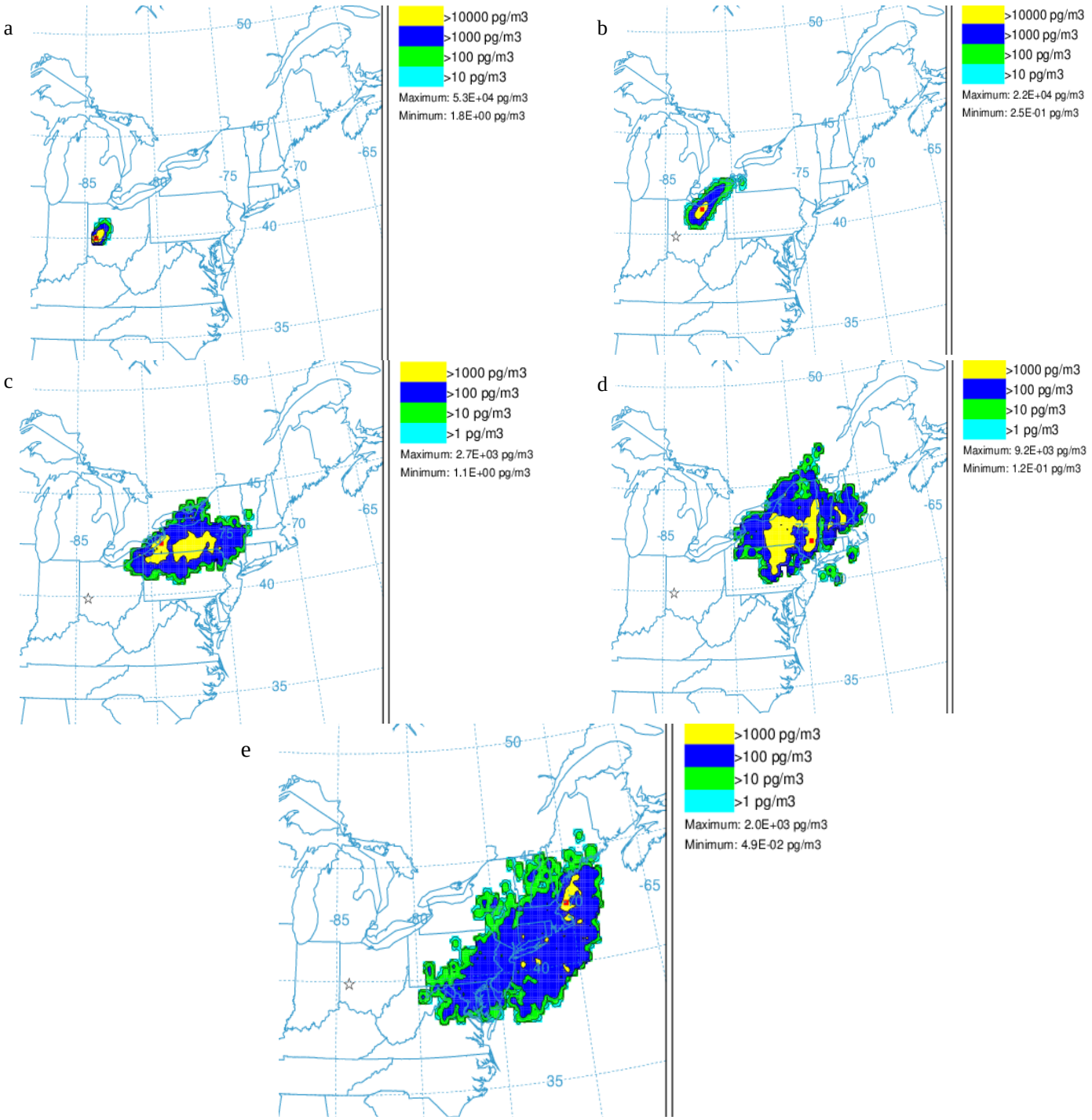

Figure 13: The Control Case: HYSPLIT representation of the PMCH cloud using the 9-km WRF and 0.25º x 0.25º concentration grid. The pollutant was released from Dayton, OH at 1705 UTC on 25 Sep 1983. The concentration distribution (in pg/m^3) is displayed in each panel with the maximum concentration location indicated by the red dot. The time steps of the panels are: 1800 UTC on 25 Sep (a), 0600 UTC on 26 Sep (b), 1800 UTC on 26 Sep (c), 0600 UTC on 27 Sep (d), and 1800 UTC on 27 Sep (e).

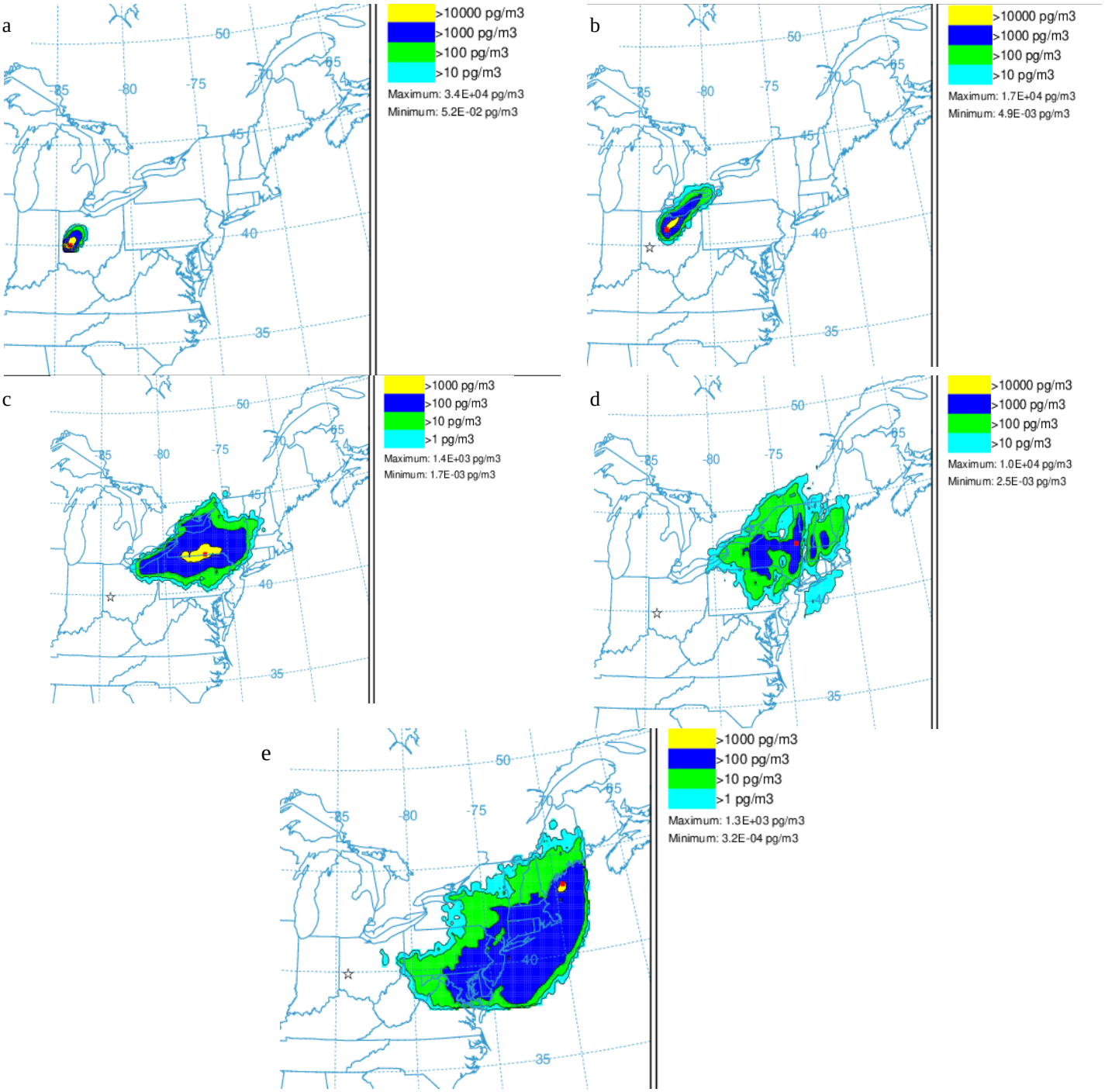

Figure 14: The Highest Ranking Case: HYSPLIT representation of the PMCH cloud using the boundary layer stability computed by the UT profile parameterization using the 9-km WRF and 0.25º x 0.25º concentration grid. The pollutant was released from Dayton, OH at 1705 UTC on 25 Sep 1983. The concentration distribution (in pg/m^3) is displayed in each panel with the maximum concentration location indicated by the red dot. The time steps of the panels are: 1800 UTC on 25 Sep (a), 0600 UTC on 26 Sep (b), 1800 UTC on 26 Sep (c), 0600 UTC on 27 Sep (d), and 1800 UTC on 27 Sep (e).

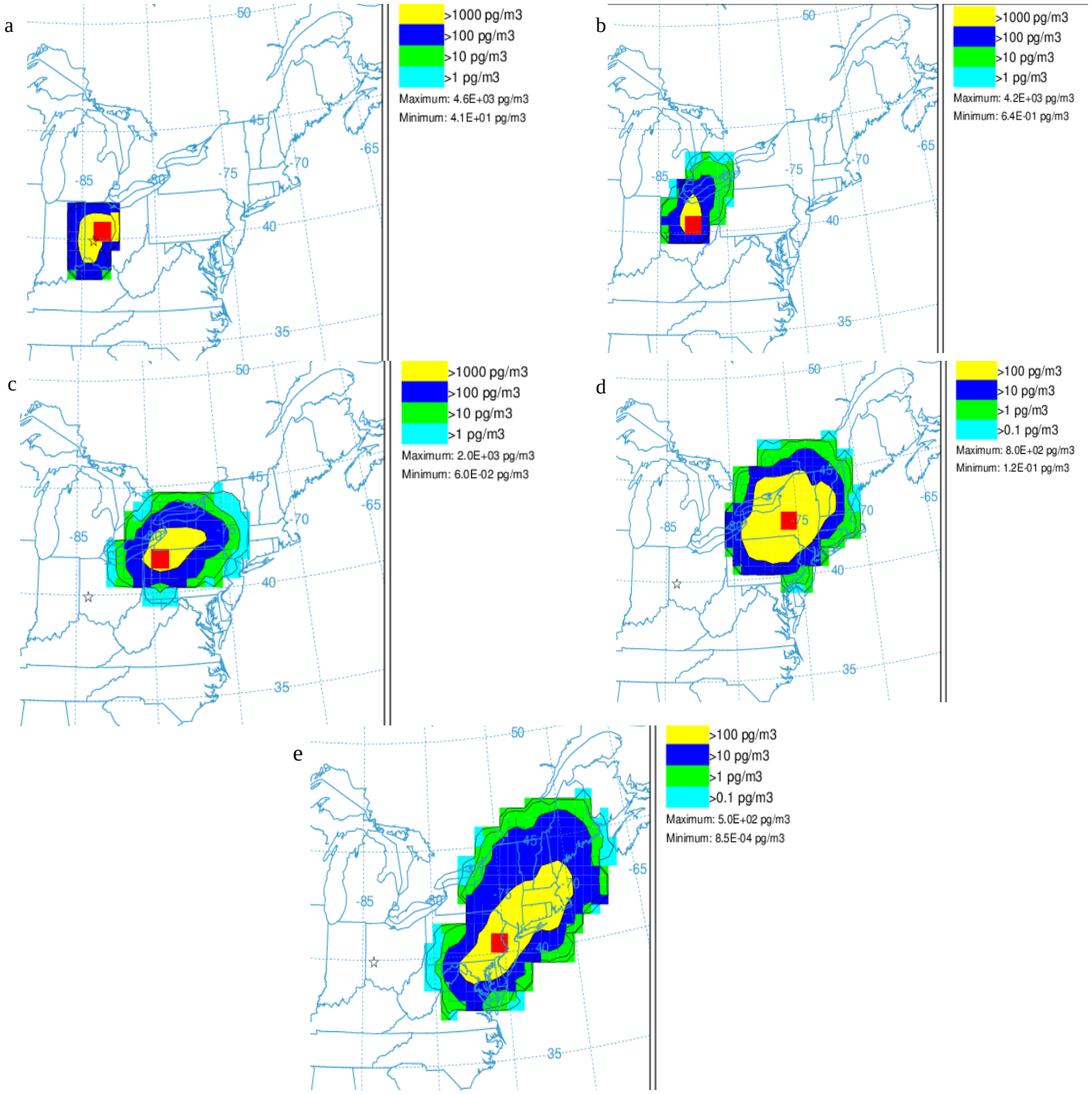

Figure 15: The Lowest Ranking Case: HYSPLIT representation of the PMCH cloud using the vertical motion determined from constant density field parameterization using the 3-km nested WRF and 1.0º x 1.0º concentration grid. The pollutant was released from Dayton, OH at 1705 UTC on 25 Sep 1983. The concentration distribution (in pg/m^3) is displayed in each panel with the maximum concentration location indicated by the red dot. The time steps of the panels are: 1800 UTC on 25 Sep (a), 0600 UTC on 26 Sep (b), 1800 UTC on 26 Sep (c), 0600 UTC on 27 Sep (d), and 1800 UTC on 27 Sep (e). The lowest ranking case here is tied to the Top Hat Particle Parameterization case (not shown).

CAPTEX Timing Spread Results

Onset timing of the predicted concentration at each station is compared to the CAPTEX measured concentrations in Figures 16 - 21. The timing error spread of all parameterization schemes in the 1.0º x 1.0º (Figures 16,17 and 18) and 0.25º x 0.25º concentration grid (Figures 19, 20, and 21) and 3-km, 9-km, and 27-km WRF runs, organized by distance away from release site (a) and elevation (b). Negative timing error indicates HYSPLIT brought plume too early to the station while positive indicates HSYPLIT brought plume too late. Across all runs, timing uncertainty increases as the plume interacts with regions of varying terrain (a). On the other hand, there is no major importance on the elevation of the station (b). Table 12 portrays the spread in onset timing at across all simulations in each set.

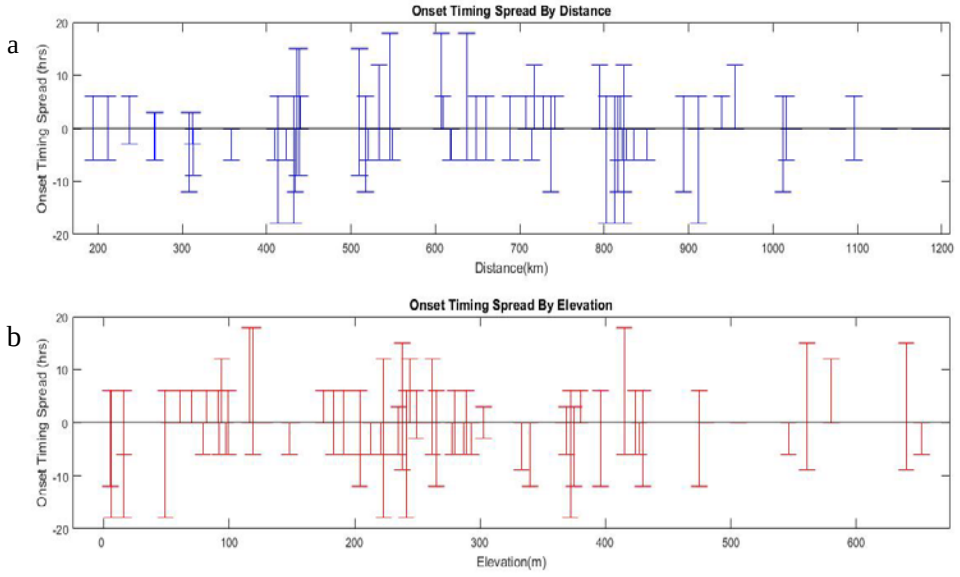

Figure 16: Onset timing spread of 1.0º x 1.0º concentration grid with 3-km WRF by distance away from release site and elevation.

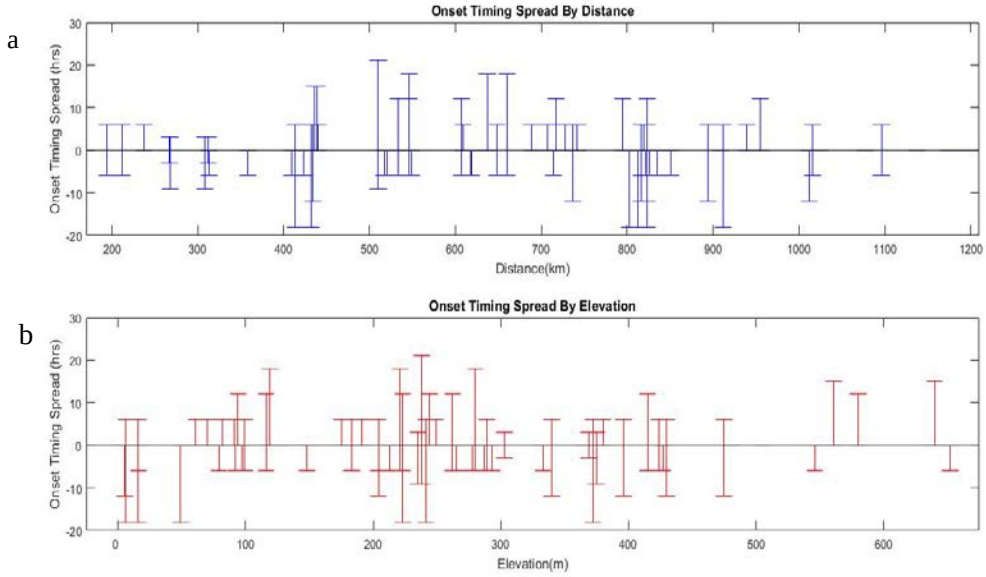

Figure 17: Onset timing spread of 1.0º x 1.0º concentration grid with 9-km WRF by distance away from release site and elevation**.**

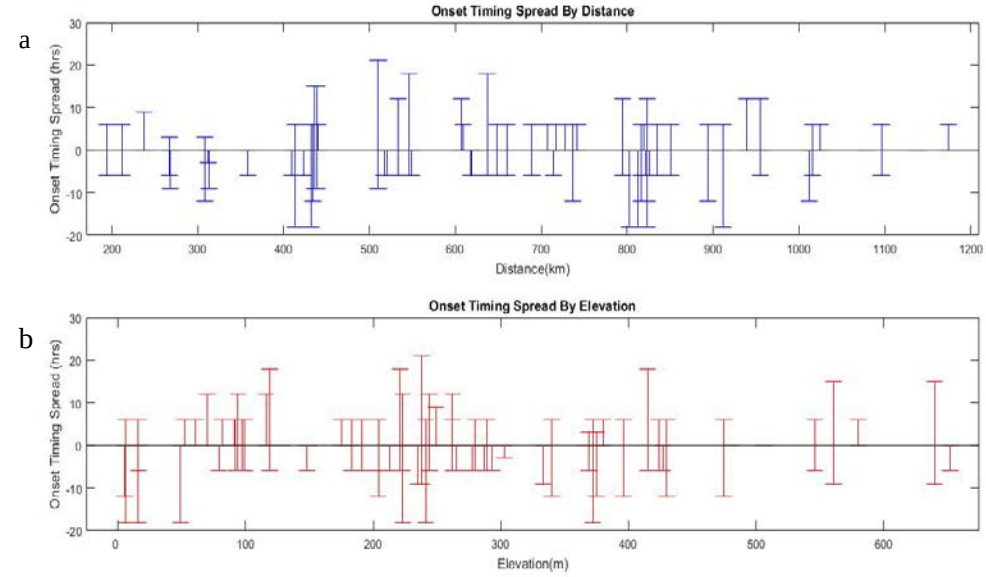

Figure 18: Onset timing spread of 1.0º x 1.0º concentration grid with 27-km WRF by distance away from release site and elevation**.**

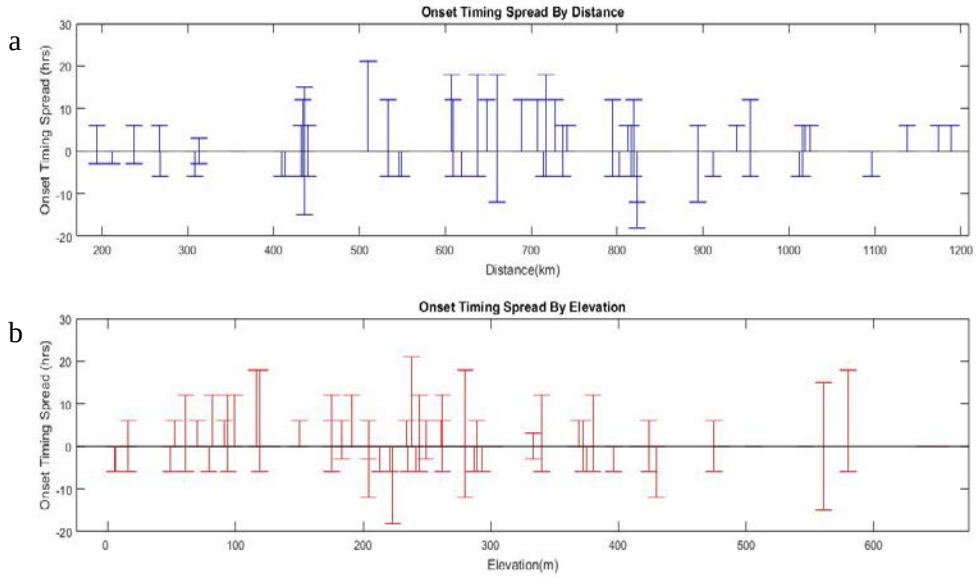

Figure 19: Onset timing spread of 0.25º x 0.25º concentration grid with 3-km WRF by distance away from release site and elevation**.**

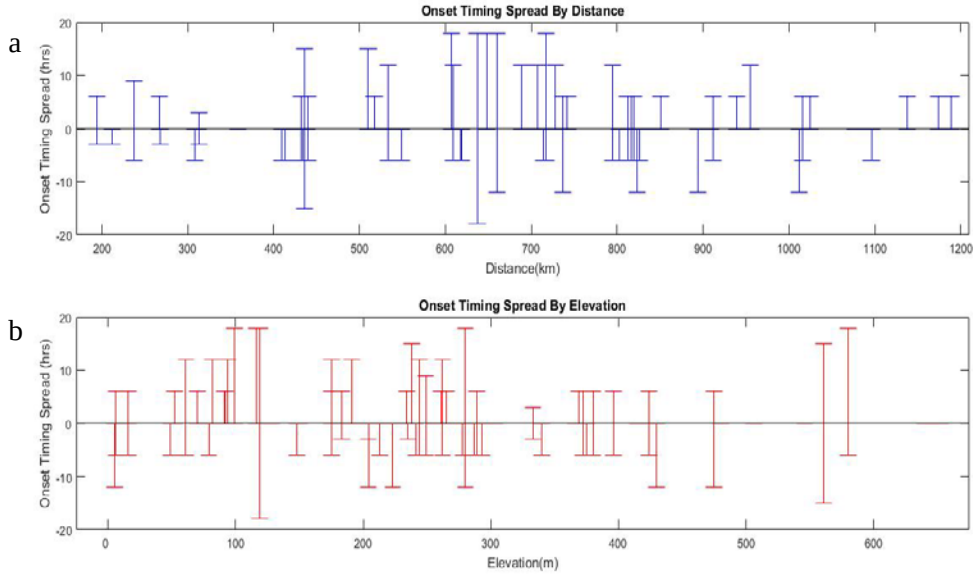

Figure 20: Onset timing spread of 0.25º x 0.25º concentration grid with 9-km WRF by distance away from release site and elevation**.**

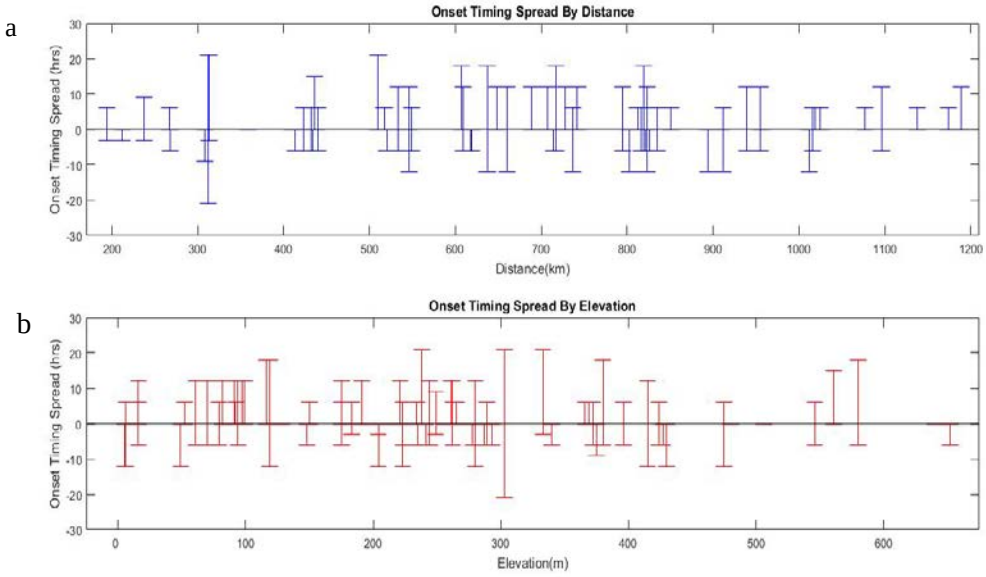

Figure 21: Timing error spread of 0.25º x 0.25º concentration grid with 27-km WRF by distance away from release site and elevation**.**

Model Onset Timing Spread	
Model Configuration	**Onset Timing Spread**
WRF 3 km & 0.25º x 0.25º Conc. Grid	-18 hrs to +21 hrs
WRF 9 km & 0.25º x 0.25º Conc. Grid	-12 hrs to +18 hrs
WRF 27 km & 0.25º x 0.25º Conc. Grid	-12 hrs to +21 hrs
WRF 3 km & 1.0º x 1.0º Conc. Grid	-18 hrs to +18 hrs
WRF 9 km & 1.0º x 1.0º Conc. Grid	-18 hrs to +21 hrs
WRF 27 km & 1.0º x 1.0º Conc. Grid	-18 hrs to +21 hrs

Table 12: Onset timing error spread across all simulations in each set. Negative timing error indicates HYSPLIT brought plume too early while positive timing error indicates HSYPLIT brought plume too late.

HYSPLIT Success Rate

A hit (successful forecast) is defined as HYSPLIT predicting PMCH concentrations greater than 0 pg/m^3 for the entire CAPTEX data set (2244 observations). HYPLIT had a plume detection success rate average of 98.07% across all runs, with the 1.0º x 1.0º concentration grid having a slightly higher rate (99.0%) compared to the 0.25º x 0.25º grid (96%), with respect to the 86 sensors. The success rate is the percentage of

observations predicted by the model compared to the measured CAPTEX data. Only concentrations greater than 0 pg/m^3 measured during the CAPTEX campaign were used.

Model Success Rate	
Model Configuration	**Percentage of Predicted vs. Measured Concentrations**
WRF 3-KM & 0.25º x 0.25º Conc. Grid	(2158/2244) 96.16%
WRF 9-KM & 0.25º x 0.25º Conc. Grid	(2159/2244) 96.21%
WRF 27-KM & 0.25º x 0.25º Conc. Grid	(2191/2244) 97.63%
WRF 3-KM & 1.0º x 1.0º Conc. Grid	(2243/2244) 99.95%
WRF 3-KM & 1.0º x 1.0º Conc. Grid	(2227/2244) 99.24%
WRF 3-KM & 1.0º x 1.0º Conc. Grid	(2228/2244) 99.28%

Table 13: HYSPLIT success rates of CAPTEX2 ensembles

Nuclear Fallout Statistical Results:

The nuclear fallout simulations saw little spread in the five statistics within each detonation. Vertical turbulence & concentration distribution have little effect on uncertainty of the plume while changes in vertical motion parameterizations have most significant effect on uncertainty. The figure of merit in space (FMS), a score that provides a quantitative measure of the overlap of the modeled and observed plume segments, is shown in Table 14. A complete list of the statistical values can be found in Appendix C.

Figure of Merit In Space Range					
Annie	***Easy***	***Harry***	***Simon***	***Smoky***	***Sugar***
70.0% - 87.5%	***58.82% - 85.29%***	***66.67% - 73.81%***	***87.27% - 92.73%***	***27.37% - 35.79%***	***65.0% - 72.5%***

Table 14: HYSPLIT FMS score spread for nuclear detonation ensembles

V. Conclusions and Recommendations

Chapter Overview:

The purpose of this chapter is to state the conclusions of this research and recommend further research to further quantify uncertainty in atmospheric transport and dispersion modeling. Conclusions are made from the analysis and results in Chapter IV above.

Conclusion of Research:

The key findings from this research are:

1. The meteorology model and its horizontal resolution have the greatest impact on uncertainty.
2. HYSPLIT's concentration grid should be determined (optimized) based on the meteorology model ingested into HYSPLIT.
3. In long range transport and dispersion, such as in the CAPTEX cases, vertical turbulence & boundary layer stability parameterizations proved fruitful in minimizing uncertainty.
4. In long range transport and dispersion, the parameterizations that have a negative impact on the transport and dispersion include: vertical motion mapped from constant density, assuming a Gaussian concentration distribution, and emissions simulated using a particle approach.
5. Timing uncertainty is greatest regions of varying terrain.
6. In nuclear cases, the figure of merit in space proved to be the most significant statistic to quantify uncertainty.

Recommendation for Future Research:

This project reveals that although there are ways to minimize and uncover uncertainty in transport and dispersion simulations there is still further research needed to fully understand and quantify uncertainty. One focus of future research is to complete an ensemble varying not only meteorology model ingested into HYSPLIT, but also finer model resolutions. The meteorological model chosen proved to have the greatest impact on uncertainty. It is recommended the meteorological model chosen be selected based on its forecasting success rate for the area of interest.

Another potential research opportunity in this field is to predict uncertainty in transport and dispersion modeling through the use of a Monte Carlo simulation. In this approach each parameter is selected either from independent distributions or from multivariate distributions specified by a covariance matrix (Rao 2005). From there the contribution of each parameter to model uncertainty is determined by statistical analysis of each simulation's results. The correlation coefficient statistics comparing each input parameter and the model output from each Monte Carlo simulation may prove to be the most relevant approach to rank each parameter's impact on the total uncertainty within the model run (Rao 2005).

Moreover, it is recommended future research should be conducted to create a Meteorology Complex Factor (MCF) to quantify the meteorology model's impact on uncertainty. This concept was first tested by Jonathan D. W. Kahl from the University of Wisconsin on his work on predicting trajectory model error (Kahl 1995). In his research the MCF describes the dispersion of stochastically generated trajectory positions compared to a reference trajectory calculation. To determine a MCF, a reference

trajectory must first be calculated. From there an ensemble of trajectories can be produced (using the Monte Carlo technique) using perturbed wind fields or varying parameterizations. The MCF could then be used to compare the stochastic (perturbed) trajectories to the reference trajectory. The perturbed wind components are computed by:

$$u_p = u + u_e \tag{45}$$

$$v_p = v + v_e \tag{46}$$

where u and v are the unperturbed horizontal wind components used to compute the initial reference trajectory and u_e and v_e are Gaussian random variables with means of zero and standard deviations of 3.0 m/s (Kahl 1995). Once an ensemble of perturbed trajectories or ensemble of varying parameterizations is completed the MCF can be calculated by:

$$MCF(t) = [\sum_i d_i(t)]/N \tag{47}$$

where $d_i(t)$ is the distance between the stochastic trajectory position at time to the reference trajectory position, and N is the number of stochastic trajectories generated (recommended 1000). A second approach to the MCF is to add the timing error across all runs within a meteorological ensemble. In this research, the researcher would add the timing error at all stations for all parameterizations in the 3-km, 9-km, and 27-km WRF runs separately (regardless of the concentration grid) and divide by the total number of runs completed using that meteorological model (60 in this research). This MCF is tested for this research using equation 48 with the results below:

$$MCF(t) = [\sum t]/N \tag{48}$$

3-kmWRF: (19,428hrs/54) = 359.77

9-km WRF: (19,683hrs/54) = 364.50

27km- WRF: (21,324hrs/54) = 394.88

The last focus for future research is to investigate further affects of vertical & horizontal turbulence and planetary boundary layer parameterizations on atmospheric transport and dispersion modeling. The turbulent eddies and motions located in the boundary layer have the most impact on the resulting motion of a pollutant. These parameterizations should be studied under various meteorological conditions to determine rules of thumb by which parameter performs the best for each weather condition.

Summary:

HYSPLIT ensembles of the CAPTEX campaign and stabilized nuclear fallout cases were useful in identifying and quantifying uncertainty in atmospheric dispersion model predictions. Uncertainty in these simulations directly linked to: 1) the meteorological model data ingested into the HYSPLIT (due to horizontal resolution and associated parameterizations), 2) HYSPLIT's internal parameterizations, and 3) the stochastic uncertainty associated with the turbulent nature of the atmosphere. Future work is required to understand these factors further and develop new ways to communicate this uncertainty.

Appendix A: Nuclear Fallout Statistics

Upshot-Knothole Simon					
Parameterization	Fractional Bias	Correlation Coefficient	Figure of Merit in Space	Kolmogorov-Smirnov Parameter	Final Rank
Isobaric	0.32	0.54	87.27	51	2.50
Isentropic	0.45	0.55	90.91	42	2.57
Constant Density	0.27	0.55	89.09	49	2.57
Isosigma	0.32	0.54	92.73	56	2.49
Divergence	0.27	0.54	92.73	54	2.54
MSL to AGL	0.27	0.57	90.91	49	2.61
Average Data	0.29	0.56	92.73	52	2.58
Damped Magnitude	0.29	0.56	92.73	52	2.58
Control Case	0.29	0.56	92.73	52	2.58
BL Stability From UT Profile	0.29	0.56	92.73	52	2.58
Vertical Mixing replaced By PBL Average	0.30	0.57	92.73	48	2.62
Vertical Turbulence Beljaars Holtslag	0.27	0.53	90.91	55	2.51
Vertical Turbulence Kanthar-Clayson	0.29	0.56	92.73	52	2.58
Vertical Turbulence From TKE Field	0.29	0.56	92.73	52	2.58
Horizontal Turbulence From Variance	0.29	0.56	92.73	52	2.58
Gaussian Horizontal Top Hat Vertical Puff	0.29	0.56	92.73	52	2.58
Top Hat Horizontal Vertical Puff	0.29	0.56	92.73	52	2.58
Gaussian Horizontal Particle Vertical	0.29	0.56	92.73	52	2.58
Top Hat Horizontal Particle Vertical	0.29	0.56	92.73	52	2.58
Puff Growth Empirical	0.29	0.56	92.73	52	2.58
Horizontal Turbulence From Velocity Deformation	0.39	0.59	96.36	51	2.61
Horizontal Turbulence Undefined – Defaulted to Velocity Deformation	0.39	0.59	96.36	51	2.61
Mixed Layer Constant at 1500m	0.29	0.53	92.73	55	2.51

Mixed Layer From Temperature	0.29	0.56	92.73	52	2.58
Mixed Layer From TKE Field	0.29	0.56	92.73	52	2.58

Plumbbob Smoky					
Parameterization	Fractional Bias	Correlation Coefficient	Figure of Merit in Space	Kolmogorov-Smirnov Parameter	Final Rank
Isobaric	-0.13	0.29	27.37	69	1.45
Isentropic	-0.10	0.19	12.63	84	1.20
Constant Density	-0.13	0.26	26.32	70	1.45
Isosigma	-0.13	0.25	26.32	70	1.45
Divergence	-0.13	0.29	27.37	70	1.44
MSL to AGL	-0.13	0.29	25.26	70	1.43
Average Data	-0.13	0.32	27.37	70	1.43
Damped Magnitude	-0.13	0.32	27.37	70	1.43
Control Case	-0.13	0.32	27.37	70	1.43
BL Stability From UT Profile	-0.13	0.32	27.37	70	1.43
Vertical Mixing replaced By PBL Average	-0.13	0.31	27.37	70	1.44
Vertical Turbulence Beljaars Holtslag	-0.13	0.31	25.26	70	1.42
Vertical Turbulence Kanthar-Clayson	-0.13	0.32	27.37	70	1.43
Vertical Turbulence From TKE Field	-0.13	0.32	27.37	70	1.43
Horizontal Turbulence From Variance	-0.13	0.32	27.37	70	1.43
Gaussian Horizontal Top Hat Vertical Puff	-0.13	0.32	27.37	70	1.43
Top Hat Horizontal Vertical Puff	-0.13	0.32	27.37	70	1.43
Gaussian Horizontal Particle Vertical	-0.13	0.32	27.37	70	1.43
Top Hat Horizontal Particle Vertical	-0.13	0.32	27.37	70	1.43
Puff Growth Empirical	-0.13	0.32	27.37	70	1.43
Horizontal Turbulence From Velocity Deformation	-0.14	0.28	35.79	61	1.63
Horizontal Turbulence Undefined – Defaulted	-0.14	0.28	35.79	61	1.63

to Velocity Deformation					
Mixed Layer Constant at 1500m	-0.13	0.31	25.26	70	1.42
Mixed Layer From Temperature	-0.13	0.32	27.37	70	1.43
Mixed Layer From TKE Field	-0.13	0.32	27.37	70	1.43

Buster-Jangle Sugar					
Parameterization	Fractional Bias	Correlation Coefficient	Figure of Merit in Space	Kolmogorov-Smirnov Parameter	Final Rank
Isobaric	-0.94	0.27	67.5	63	1.65
Isentropic	-1.05	0.24	72.5	63	1.63
Constant Density	-0.98	0.28	67.5	63	1.63
Isosigma	-0.99	0.25	67.5	63	1.61
Divergence	-0.95	0.27	67.5	65	1.62
MSL to AGL	-0.99	0.22	62.5	60	1.58
Average Data	-1.03	0.21	67.5	63	1.57
Damped Magnitude	-1.03	0.21	67.5	63	1.57
Control Case	-1.03	0.21	67.5	63	1.57
BL Stability From UT Profile	-1.03	0.21	67.5	63	1.57
Vertical Mixing replaced By PBL Average	-1.03	0.24	65	63	1.56
Vertical Turbulence Beljaars Holtslag	-0.99	0.24	65	63	1.61
Vertical Turbulence Kanthar-Clayson	-1.03	0.21	67.5	63	1.57
Vertical Turbulence From TKE Field	-1.03	0.21	67.5	63	1.57
Horizontal Turbulence From Variance	-1.03	0.21	67.5	63	1.57
Gaussian Horizontal Top Hat Vertical Puff	-1.03	0.21	67.5	63	1.57
Top Hat Horizontal Vertical Puff	-1.03	0.21	67.5	63	1.57
Gaussian Horizontal Particle Vertical	-1.03	0.21	67.5	63	1.57
Top Hat Horizontal Particle Vertical	-1.03	0.21	67.5	63	1.57
Puff Growth Empirical	-1.03	0.21	67.5	63	1.57

Horizontal Turbulence From Velocity Deformation	-1.04	0.26	67.5	63	1.59
Horizontal Turbulence Undefined – Defaulted to Velocity Deformation	-1.04	0.26	67.5	63	1.59
Mixed Layer Constant at 1500m	-1.00	0.21	67.5	63	1.59
Mixed Layer From Temperature	-1.03	0.21	67.5	63	1.57
Mixed Layer From TKE Field	-1.03	0.21	67.5	63	1.57

Tumbler-Snapper Easy					
Parameterization	Fractional Bias	Correlation Coefficient	Figure of Merit in Space	Kolmogorov-Smirnov Parameter	Final Rank
Isobaric	0.15	0.73	85.29	50	2.81
Isentropic	-0.31	0.56	58.82	56	2.19
Constant Density	0.15	0.72	85.29	53	2.77
Isosigma	0.11	0.72	85.29	53	2.79
Divergence	0.16	0.73	85.29	53	2.78
MSL to AGL	0.01	0.71	85.29	59	2.76
Average Data	0.06	0.71	85.29	59	2.74
Damped Magnitude	0.06	0.71	85.29	59	2.74
Control Case	0.06	0.71	85.29	59	2.74
BL Stability From UT Profile	0.06	0.71	85.29	59	2.74
Vertical Mixing replaced By PBL Average	0.06	0.71	85.29	59	2.74
Vertical Turbulence Beljaars Holtslag	0.01	0.72	85.29	59	2.77
Vertical Turbulence Kanthar-Clayson	0.06	0.71	85.29	59	2.74

Vertical Turbulence From TKE Field	0.06	0.71	85.29	59	2.74
Horizontal Turbulence From Variance	0.06	0.71	85.29	59	2.74
Gaussian Horizontal Top Hat Vertical Puff	0.06	0.71	85.29	59	2.74
Top Hat Horizontal Vertical Puff	0.06	0.71	85.29	59	2.74
Gaussian Horizontal Particle Vertical	0.06	0.71	85.29	59	2.74
Top Hat Horizontal Particle Vertical	0.06	0.71	85.29	59	2.74
Puff Growth Empirical	0.06	0.71	85.29	59	2.74
Horizontal Turbulence From Velocity Deformation	0.01	0.72	85.29	56	2.81
Horizontal Turbulence Undefined – Defaulted to Velocity Deformation	0.01	0.72	85.29	56	2.81
Mixed Layer Constant at 1500m	0.04	0.71	85.29	56	2.77
Mixed Layer From Temperature	0.06	0.71	85.29	59	2.74
Mixed Layer From TKE Field	0.06	0.71	85.29	59	2.74

Upshot-Knothole Annie					
Parameterization	Fractional Bias	Correlation Coefficient	Figure of Merit in Space	Kolmogorov-Smirnov Parameter	Final Rank
Isobaric	-0.28	-0.21	77.50	35	2.33
Isentropic	-0.19	-0.23	70.00	43	2.23
Constant Density	-0.24	-0.21	77.50	40	2.30
Isosigma	-0.24	-0.21	77.50	37	2.33
Divergence	-0.29	-0.21	77.50	37	2.30
MSL to AGL	-0.21	-0.22	77.50	37	2.35
Average Data	-0.18	-0.22	77.50	35	2.38
Damped Magnitude	-0.18	-0.22	77.50	35	2.38
Control Case	-0.18	-0.22	77.50	35	2.38
BL Stability From UT Profile	-0.18	-0.22	77.50	35	2.38

Vertical Mixing replaced By PBL Average	-0.26	-0.22	77.50	38	2.31
Vertical Turbulence Beljaars Holtslag	-0.25	-0.21	80.00	35	2.37
Vertical Turbulence Kanthar-Clayson	-0.18	-0.22	77.50	35	2.38
Vertical Turbulence From TKE Field	-0.18	-0.22	77.50	35	2.38
Horizontal Turbulence From Variance	-0.18	-0.22	77.50	35	2.38
Gaussian Horizontal Top Hat Vertical Puff	-0.18	-0.22	77.50	35	2.38
Top Hat Horizontal Vertical Puff	-0.18	-0.22	77.50	35	2.38
Gaussian Horizontal Particle Vertical	-0.18	-0.22	77.50	35	2.38
Top Hat Horizontal Particle Vertical	-0.18	-0.22	77.50	35	2.38
Puff Growth Empirical	-0.18	-0.22	77.50	35	2.38
Horizontal Turbulence From Velocity Deformation	-0.25	-0.21	87.50	33	2.46
Horizontal Turbulence Undefined – Defaulted to Velocity Deformation	-0.25	-0.21	87.50	33	2.46
Mixed Layer Constant at 1500m	-0.26	-0.21	77.50	38	2.31
Mixed Layer From Temperature	-0.18	-0.22	77.50	35	2.38
Mixed Layer From TKE Field	-0.18	-0.22	77.50	35	2.38

Upshot-Knothole Harry					
Parameterization	Fractional Bias	Correlation Coefficient	Figure of Merit in Space	Kolmogorov-Smirnov Parameter	Final Rank
Isobaric	-0.97	-0.11	72.62	40	1.85
Isentropic	-1.05	-0.14	67.86	46	1.72
Constant Density	-0.94	-0.13	73.81	40	1.88
Isosigma	-0.97	-0.12	70.24	42	1.82
Divergence	-0.98	-0.13	66.67	42	1.77
MSL to AGL	-0.96	-0.12	73.81	42	1.85
Average Data	-1.00	-0.11	67.86	42	1.77

Damped Magnitude	-1.00	-0.11	67.86	42	1.77
Control Case	-1.00	-0.11	67.86	42	1.77
BL Stability From UT Profile	-1.00	-0.11	67.86	42	1.77
Vertical Mixing replaced By PBL Average	-0.97	-0.12	66.67	42	1.78
Vertical Turbulence Beljaars Holtslag	-1.00	-0.13	65.48	42	1.75
Vertical Turbulence Kanthar-Clayson	-1.00	-0.11	67.86	42	1.77
Vertical Turbulence From TKE Field	-1.00	-0.11	67.86	42	1.77
Horizontal Turbulence From Variance	-1.00	-0.11	67.86	42	1.77
Gaussian Horizontal Top Hat Vertical Puff	-1.00	-0.11	67.86	42	1.77
Top Hat Horizontal Vertical Puff	-1.00	-0.11	67.86	42	1.77
Gaussian Horizontal Particle Vertical	-1.00	-0.11	67.86	42	1.77
Top Hat Horizontal Particle Vertical	-1.00	-0.11	67.86	42	1.77
Puff Growth Empirical	-1.00	-0.11	67.86	42	1.77
Horizontal Turbulence From Velocity Deformation	-0.98	-0.13	73.81	43	1.83
Horizontal Turbulence Undefined – Defaulted to Velocity Deformation	-0.98	-0.13	73.81	43	1.83
Mixed Layer Constant at 1500m	-0.99	-0.12	70.24	43	1.79
Mixed Layer From Temperature	-1.00	-0.11	67.86	42	1.77
Mixed Layer From TKE Field	-1.00	-0.11	67.86	42	1.77

Bibliography

Air Resources Laboratory, 2018: HYSPLIT Basic Tutorial. Accessed 15 Oct 2018 , https://ready.arl.noaa.gov/documents/Tutorial/html/index.html.

Beljaars, A.C.M., and A.K. Betts, 1993: Estimation of effective roughness length for heat and momentum from FIFE data. *Atmos. Res.* **30,** 251-261.

Beljaars, A.C.M., and A.A.M. Holtslag, 1991: Flux parameterizations over land surfaces for atmospheric models. *J. Appl. Meteorol*., **30**, 327-341.

Coniglio, M.C., 2012: Verification of RUC0-1-h forecasts and SPC mesoscale analyses using VORTEX2 soundings. *Wea. Forecasting,* **27,** 667-683, doi:10.1175/WAF-D-11-00096.1.

Deardorff, J.W., 1973: The use of subgrid transport equations in a three-dimensional model of atmospheric turbulence, *J. Fluids Eng.*, **95**, 429-438.

Draxler, R.R., 1982: Measuring and modeling the transport and dispersion of kRYPTON-85 1500 km from a point source. *Atmos. Env.* (1967) **16**(12), 2763-2776. http://dx.doi.org/10.1016/0004-6981(82)90027-0.

Draxler, R. R., and G. D. Hess, 1998: An Overview of the HYSPLIT 4 Modelling System for Trajectories, Dispersion, and Deposition. *Aust. Meteor. Mag.* **47,** 295-308.

Draxler, R. R., and G. D. Hess, 2018: Description of the HYSPLIT 4 Modeling System. Tech. Accessed 15 Oct 2018., https://www.arl.noaa.gov/documents/reports/arl-224.pdf.

Earth System Research Laboratory. 2019: 6-Hourly NCEP/NCAR Reanalysis Data Composites. Accessed 31 Dec 2018, https://www.esrl.noaa.gov/psd/data/composites/hour/

Ferber, G. J., J. L. Heffter, R. R. Draxler, R. J. Lagomarsino, F. L. Thomas, R. N. Dietz, and C. M. Benkovitz, 1986: Cross-Appalachian Tracer Experiment (CAPTEX ’83) Final Report. NOAA Tech. Memo. ERL ARL-142, Air Resources Laboratory, NOAA Environmental Research Laboratories, Silver Spring, Maryland 20910.

Heffter, J.L., and B.J.B. Stunder, 1993: Volcanic ash forecast transport and dispersion (VAFTD) model, *Wea. Forecasting*, **8,** 533-541.

Holtslag, A.A.M., and B.A. Boville, 1993: Local versus nonlocal boundary-layer diffusion in a global climate model. *J. Climate*, 6, 1825-1842.

Hong. S.-Y., and H.-L. Pan, 1996: Nonlocal boundary layer vertical diffusion in a medium-range forecast model. *Mon. Wea. Rev.*, **124,** 2322-2339, doi:10.1175/1520-0493(1996)124<NBLVDI>2.0CO;2.

Kadar, B.A. and V.G. Perepelkin, 1989: Effect of the unstable stratification on wind and temperature profiles in the surface layer. *Atmos. Oceanic Phys*., **25**, 583-588.

Kahl, J.D.W., 1996: On the prediction of trajectory model error. *Atmos. Environ.*, **30,** 2945-2957.

Kahl, J.D., and P.J. Samson, 1988: Uncertainty in estimating boundary-layer transport during highly convective conditions. *J. Appl. Meteor.* **27,** 1024-1035.

NATO, 2010. Warning and Reporting and Hazard Prediction of Chemical, Biological, Radiological and Nuclear Incidents (Operators Manual). NATO/PfP UNCLASSIFIED, ATP – 45 (D). http://www.assistdocs.com/search/document_details.cfm?ident_number=97673.

Rolph, G.D., F. Ngan, and R.R. Draxler, 2014: Modeling the fallout from stabilized nuclear clouds using the HYSPLIT atmospheric dispersion model. *J. Environ. Radioact.,* **136,** 41-55.

Smagorinsky, J., 1963: General circulation experiments with the primitive equations: 1. The basic experiment, Mon.Weath. Rev.,**91** 99-164

Stein, A. F., R. R. Draxler, G. D. Rolph, B. J. Stunder, M. D. Cohen, and F. Ngan, 2015: NOAA's HYSPLIT Atmospheric Transport and Dispersion Modeling System. *Bull. Amer. Meteor. Soc.*,**96**(12), 2059–2077, doi:10.1175/BAMS-D-14-00110.1

Stensrud, D.J., 2007: Parametrization schemes: Keys to understanding numerical weather prediction models. Cambridge University Press.

Troen, I., and L. Mahrt, 1986: A simple model of the atmospheric boundary layer: sensitivity to surface evaporation. *Bound-Layer Meteor.*, **37,** 129-148.

Warner, T.T., 2011: Numerical weather and climate prediction. Cambridge University Press.

Weseley, M.L 1989: Parameterization of Surface Resistances to Gaseous Dry Deposition in Regional-Scale Numerical Models. *Atmos. Environ.* **23**(6), 1293-1304.

Zoellick, C., 2018: Source Term Estimation of Atmospheric Pollutants Using an Ensemble of HYSPLIT Concentration Simulations. Master's Thesis, Air Force Institute of Technology.

REPORT DOCUMENTATION PAGE

Form Approved
OMB No. 074-0188

1. REPORT DATE *(DD-MM-YYYY)*	**2. REPORT TYPE**	**3. DATES COVERED** *(From – To)*
26-02-2019	Master's Thesis	October 2017 – March 2019

TITLE AND SUBTITLE
QUANTIFYING UNCERTAINTY OF ENSEMBLE TRANSPORT AND DISPERSION SIMULATIONS USING HYSPLIT

5a. CONTRACT NUMBER

5b. GRANT NUMBER

5c. PROGRAM ELEMENT NUMBER

6. AUTHOR(S)

Bazemore, Daniel W., Captain, USAF

5d. PROJECT NUMBER

5e. TASK NUMBER

5f. WORK UNIT NUMBER

7. PERFORMING ORGANIZATION NAMES(S) AND ADDRESS(S)
Air Force Institute of Technology
Graduate School of Engineering and Management (AFIT/ENY)
2950 Hobson Way, Building 640
WPAFB OH 45433-7765

8. PERFORMING ORGANIZATION REPORT NUMBER
AFIT-ENP-MS-19-M-065

9. SPONSORING/MONITORING AGENCY NAME(S) AND ADDRESS(ES)
Air Force Technical Applications Center
1201 Edward H. White Ste. C-129
Patrick AFB, FL 32925
COMM 321-853-8410
Email: William.Roeder@us.af.mil

10. SPONSOR/MONITOR'S ACRONYM(S)
AFTAC

11. SPONSOR/MONITOR'S REPORT NUMBER(S)

12. DISTRIBUTION/AVAILABILITY STATEMENT
DISTRUBTION STATEMENT A:
APPROVED FOR PUBLIC RELEASE; DISTRIBUTION UNLIMITED.

13. SUPPLEMENTARY NOTES

14. ABSTRACT

Uncertainty associated with determining the source location of nuclear pollutants in the atmosphere after a nuclear fallout using a numerical model is difficult to determine. Uncertainty can originate from input data (meteorological and emissions), internal model error, physics parameterizations, and stochastic processes. This study uses the Hybrid Single Particle Lagrangian Integrated Trajectory (HYSPLIT) model with data from the 1983 Cross Appalachian Tracer Experiment (CAPTEX) (Ferber et al. 1986) and simulating six nuclear detonations (Rolph et al. 2014) to quantify and communicate uncertainty in ensemble dispersion simulations. This is accomplished by utilizing an ensemble of forward trajectory simulations varying initial conditions and physical parameterizations (e.g. turbulence, boundary layer stability and mixed layer depth). The model rank for each simulation is calculated using ground measurements. This value is compared against the observed rank from the CAPTEX experiment to measure the sensitivity of each model run. Effectively quantifying and communicating uncertainty is crucial in providing probabilistic results in nuclear monitoring.

15. SUBJECT TERMS
Atmospheric Transport and Dispersion, HYSPLIT, Uncertainty

16. SECURITY CLASSIFICATION OF:			**17. LIMITATION OF ABSTRACT**	**18. NUMBER OF PAGES**	**19a. NAME OF RESPONSIBLE PERSON**
a. REPORT	**b. ABSTRACT**	**c. THIS PAGE**			Maj H.R. Tseng, AFIT/ENP
U	**U**	**U**	**U**	82	**19b. TELEPHONE NUMBER** *(Include area code)* (937) 255-3636, ext 4520 hsien-liang.tseng@afit.edu

Standard Form 298 (Rev. 8-98)
Prescribed by ANSI Std. Z39-18